NAVAL POSTGRADUATE SCHOOL
Monterey, California

THESIS

A STUDY OF PRECIPITATION OCCURRENCE
USING VISUAL AND INFRARED SATELLITE DATA

by

Linda Sue Paul

December 1983

Thesis Advisor: C. H. Wash

Approved for public release; distribution unlimited.

REPORT DOCUMENTATION PAGE

READ INSTRUCTIONS BEFORE COMPLETING FORM

1. REPORT NUMBER	2. GOVT ACCESSION NO. / 3. RECIPIENT'S CATALOG NUMBER
4. TITLE (and Subtitle): A Study of Precipitation Occurrence using Visual and Infrared Satellite Data	5. TYPE OF REPORT & PERIOD COVERED: Master's Thesis December 1983
	6. PERFORMING ORG. REPORT NUMBER
7. AUTHOR(s): Linda Sue Paul	8. CONTRACT OR GRANT NUMBER(s)
9. PERFORMING ORGANIZATION NAME AND ADDRESS: Naval Postgraduate School, Monterey, California 93943	10. PROGRAM ELEMENT, PROJECT, TASK AREA & WORK UNIT NUMBERS
11. CONTROLLING OFFICE NAME AND ADDRESS	12. REPORT DATE: December 1983
	13. NUMBER OF PAGES: 114
14. MONITORING AGENCY NAME & ADDRESS (if different from Controlling Office)	15. SECURITY CLASS. (of this report)
	15a. DECLASSIFICATION/DOWNGRADING SCHEDULE

16. DISTRIBUTION STATEMENT (of this Report)

Approved for public release; distribution unlimited

17. DISTRIBUTION STATEMENT (of the abstract entered in Block 20, if different from Report)

18. SUPPLEMENTARY NOTES

19. KEY WORDS (Continue on reverse side if necessary and identify by block number)

Satellite Precipitation Specification
Satellite Meteorology
Bi-spectral Satellite Threshold
Objective Forecasting

20. ABSTRACT (Continue on reverse side if necessary and identify by block number)

Bi-spectral satellite thresholds for precipitation specification are explored with visual and infrared satellite data collocated with Service-A hourly observations for 137 surface stations in the southeastern United States. The data span the month of August 1979 and total 70,623 observations, including 538 daylight precipitation observations.

The distributional and statistical differences of four satellite resolution sizes ranging from 484 to 2025 nmi^2 are

(20. ABSTRACT continue)

explored and determined to be significant in the representation of weather conditions. Precipitation and no-precipitation data can be statistically differentiated with the visual and infrared mean and standard deviation values.

For overcast ceiling reports, a simple linear bi-spectral threshold based on a 50% probability of precipitation is defined as extending from albedo 1.00 to 0.60 with associated cloud top temperatures 290K and 210K, respectively. For overcast and broken ceiling reports, an albedo greater than 0.80 specifies a 50% probability of precipitation.

Approved for public release; distribution unlimited

A Study of Precipitation Occurrence using Visual and Infrared Satellite Data

by

Linda Sue Paul
Lieutenant, United States Navy
B. S., University of Minnesota, 1977

Submitted in partial fulfillment of the requirements for the degree of

MASTER OF SCIENCE IN METEOROLOGY AND OCEANOGRAPHY

from the

NAVAL POSTGRADUATE SCHOOL
December 1983

ABSTRACT

Bi-spectral satellite thresholds for precipitation specification are explored with visual and infrared satellite data collocated with Service-A hourly observations for 137 surface stations in the southeastern United States. The data span the month of August 1979 and total 70,623 observations, including 538 daylight precipitation observations.

The distributional and statistical differences of four satellite resolution sizes ranging from 484 to 2025 nmi^2 are explored and determined to be significant in the representation of weather conditions. Precipitation and no-precipitation data can be statistically differentiated with the visual and infrared mean and standard deviation values.

For overcast ceiling reports, a simple linear bi-spectral threshold based on a 50% probability of precipitation is defined as extending from albedo 1.00 to 0.60 with associated cloud top temperatures 290K and 210K, respectively. For overcast and broken ceiling reports, an albedo greater than 0.80 specifies a 50% probability of precipitation.

TABLE OF CONTENTS

LIST OF FIGURES

LIST OF TABLES

I. INTRODUCTION

The determination of precipitation occurrence and amounts is an important factor in scientific, commercial, and operational endeavors. Scientific uses are concentrated in the fields of meteorology, hydrology, and oceanography, where precipitation is essential in analysis, diagnosis, prediction, and verification. Within meteorology, precipitation serves as both a forcing and response element in the study of daily weather and climatology. Indeed, precipitation is a critical input for climate research and into general circulation models which promise to extend the time frame of skillful weather forecasts. Commercial uses encompass agriculture, forestry, transportation, communications, water resource management, and many others.

Despite the importance of precipitation data to a variety of fields, there are serious shortcomings in current precipitation determination. These shortcomings are due to areal and economic limitations imposed upon the land-based rainfall monitoring systems. A possible solution is embodied in precipitation information extracted from satellite data. With the advent of high resolution, multi-spectral channel satellites in the late 1970's, satellite derived

precipitation data are being studied as a viable method to complement and supplement conventional rainfall data.

The satellite image interpreter does a subjective analysis based on the gray shade variations, representing a range of digital counts, that appear in the satellite image. However, satellite data contain more information within the digital values than can be resolved by the human eye in photographic images. The satellite digital counts input into a computer allow use of the full range of the digital values.

Until recently, computer processing of satellite data has been confined largely to research uses. Acquisition, storage, and processing of the huge volumes of digital satellite data could not be handled operationally in real time. However, with the recent advent of more capable mini-computer systems, such as the United States Navy's Satellite Data Processing And Display System (SPADS) developed by the Naval Environmental Prediction Research Facility (NEPRF) Monterey, California, real time quantitative use of digital satellite data has become a reality. With the operational availability of such systems as the SPADS unit, there is a need for numerical schemes to aid in the objective specification of current weather conditions.

This thesis concentrates on the specification of visual and infrared satellite data thresholds in determining precipitation occurrence and qualitative precipitation rates in a mid-latitude coastal environment. The data set used consists of collocated Geostationary Operational Environmental Satellite--East (GOES-E) satellite data and hourly surface observations at East Coast and Gulf Coast United States stations, south of 40°N, for the month of August 1979.

The use of satellite data for precipitation specification is not new. There is the recognized limitation that infrared and visual satellite sensors are measuring properties associated with small cloud particles and not precipitation sized particles. Nonetheless, Muench and Keegan (1979) specified quantitative precipitation rates, Liljas (1981a, 1981b) specified qualitative precipitation rates, and Lovejoy and Austin (1979) delineated rain versus no-rain cases using visual and infrared satellite data. Del Beato (1981) used cloud top temperatures within a restricted cloud case classification to derive qualitative precipitation rates.

The currently available precipitation study results are based on data sets with region, season, and size

limitations. This research effort will use data from stations covering more than 420,000 square nautical miles (nmi^2) in the eastern and central United States with a total of 70,623 observations (538 precipitation observations). In comparison, the relatively comprehensive precipitation study of Muench and Keegan (1979) was based on 552 cases (300 rainfall cases) from five stations in the northeastern United States for April through November 1977. The significantly larger size of the present sample will allow better statistical determination of appropriate distributions and threshold value significance.

The primary objective of this thesis is to investigate specification of precipitation versus no-precipitation from satellite visible and infrared digital counts. Additionally, in precipitation cases, the feasibility of qualitative specification of light versus moderate/heavy precipitation and quantiative specification of convective versus continuous precipitation are investigated.

The thesis is organized into five chapters. Chapter II reviews the satellite data based precipitation studies. Chapter III describes the data set, the data processing and the testing program. Chapter IV describes the results.

Chapter V states the conclusions and suggests further research.

II. PRECIPITATION SPECIFICATION

A. INTRODUCTION

The specification of precipitation and the estimation of rainfall rates using satellite imagery have been studied using a variety of methods over a wide spectrum of time scales. This review will concentrate on those methods developed for synoptic scale and mesoscale analysis of precipitation on a diurnal or shorter time scale. The methods reviewed include bi-spectral and infrared threshold (Muench and Keegan, 1979; Liljas, 1981a, 1981b; Lovejoy and Austin, 1979; Del Beato, 1981; Wylie, 1982) and life history (Scofield, 1981; Griffith et al., 1978; Stout et al., 1979; Wylie, 1979; Negri and Adler, 1981).

B. BI-SPECTRAL AND INFRARED THRESHOLD

The bi-spectral threshcld method, in which infrared and visual satellite data are used, involves mapping the extent and distribution of precipitation. Combining the visual and infrared data provides information on the cloud temperatures (infrared data) and on the cloud thickness (visual data). Thus, while use of the visual or infrared data alone may

have limitations in specifying precipitation, the combination of both may succeed at specifying precipitation. The multi-spectral satellite channels introduced on satellites in the late 1970's yielded the possibility of bi-spectral thresholds. Threshold values and study condition parameters of selected bi-spectral studies are summarized in Table I.

TABLE I

Summary of Bi-spectral and Infrared Threshold Values

STUDY	LOCATION	CASES	TIME OF YEAR	THRESHOLD VALUE INFRARED	VISUAL
Muench and Keegan (1979)	Northeastern United States	552 observations	April-November 1977	-12°C	0.60
Liljas (1981)	Scandinavia	-	May 1979 August 1979	-12°C to -15°C	-
Lovejoy and Austin (1979)	Montreal	17 days	June 1977	-21°C, -26°C, -41°C	.80, .88*

* Visual threshold based on normalized scale from 0 - 1

Muench and Keegan (1979) studied precipitation specification using GOES visual and infrared satellite data and hourly rainfall climatological data for five stations in the northeastern United States for the period April through November 1977. Their data set consisted of 552

observations, comprised of 300 rainfall observations and 252 cases of either nonprecipitating cloudy or fair weather observations. The visual (1 km resolution) and infrared (7 km resolution) satellite data were area averaged over 7 x 7 square kilometers (km^2) and 14 x 14 km^2, respectively. A 65 point visual data array (8 x 8 plus the center point) and a 17 point infrared data array (4 x 4 plus the center point) were centered over each station. The GOES visual data were normalized using reflection values from Liou (1976) with the modification of lower absorption and higher transmission to compensate for Liou's treatment of the complete solar spectrum. The anisotropic radiation of clouds was corrected with functions calculated by Muench and Keegan (1979) from ground-based radiometers and satellite measurements. From these data, they determined probabilities for precipitation greater than .01 and .10 inches in one hour and the amount of precipitation for the hour following the satellite observation (see Figs. 1, 2, and 3).

Muench and Keegan (1979) did not provide the standard deviations for the data in these figures. However, they stated there was "considerable uncertainty in the specification of rainfall amount." As an example, they stated that

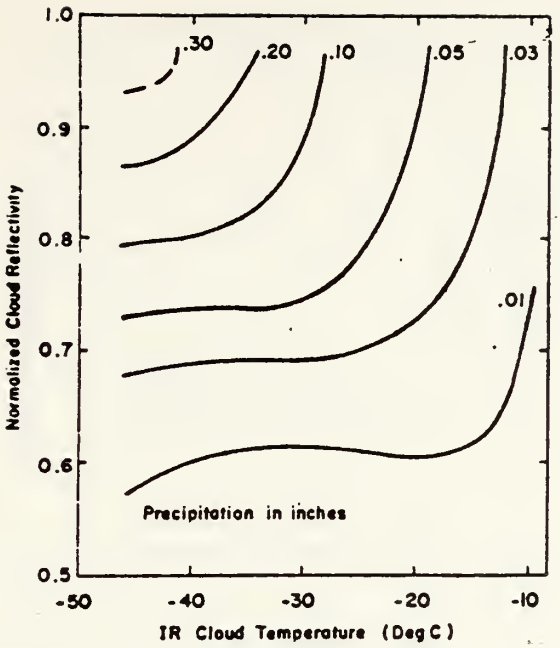

Figure 1. One-hour Rainfall as a Function of Normalized Cloud Reflectivity and Infrared Cloud Temperature (from Muench and Keegan, 1979)

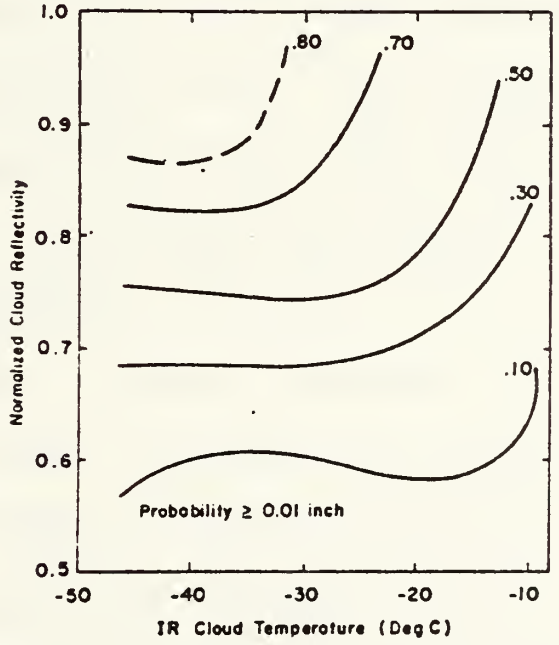

Figure 2. Probability of One-hour Rainfall Greater than or Equal to 0.01 inches as a Function of Cloud Reflectivity and Infrared Cloud Temperature (from Muench and Keegan, 1979)

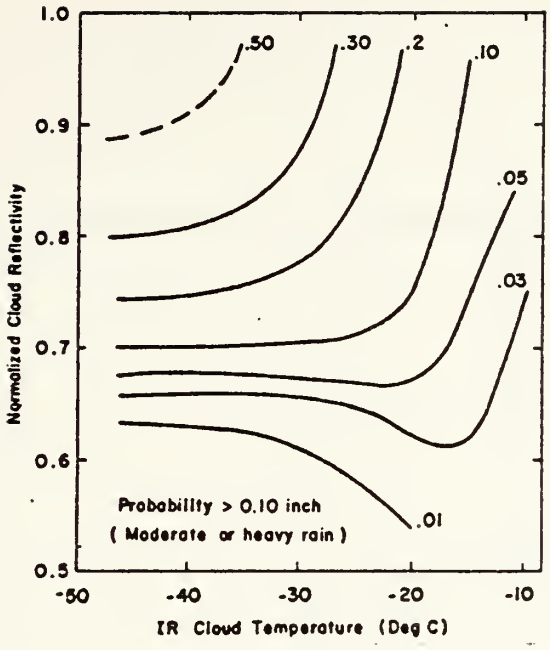

Figure 3. Probability of One-hour Rainfall Greater than 0.10 Inches as a Function of Cloud Reflectivity and Infrared Cloud Temperature (from Muench and Keegan, 1979)

using Fig. 3 "for a one-hour rainfall specification of 0.10, two-thirds of the values would fall between 0.25 and 0.04." Muench and Keegan stated that their figures emphasize the requirement for both visual and infrared data to specify precipitation amounts.

Liljas (1981a, 1981b) developed a bi-spectral cloud classification based on visual and infrared data from the polar orbiting TIROS--6 satellite (see Fig. 4 and Table II). The data set consisted of a limited number of daily observations, chosen for their synoptic characteristics, in May and

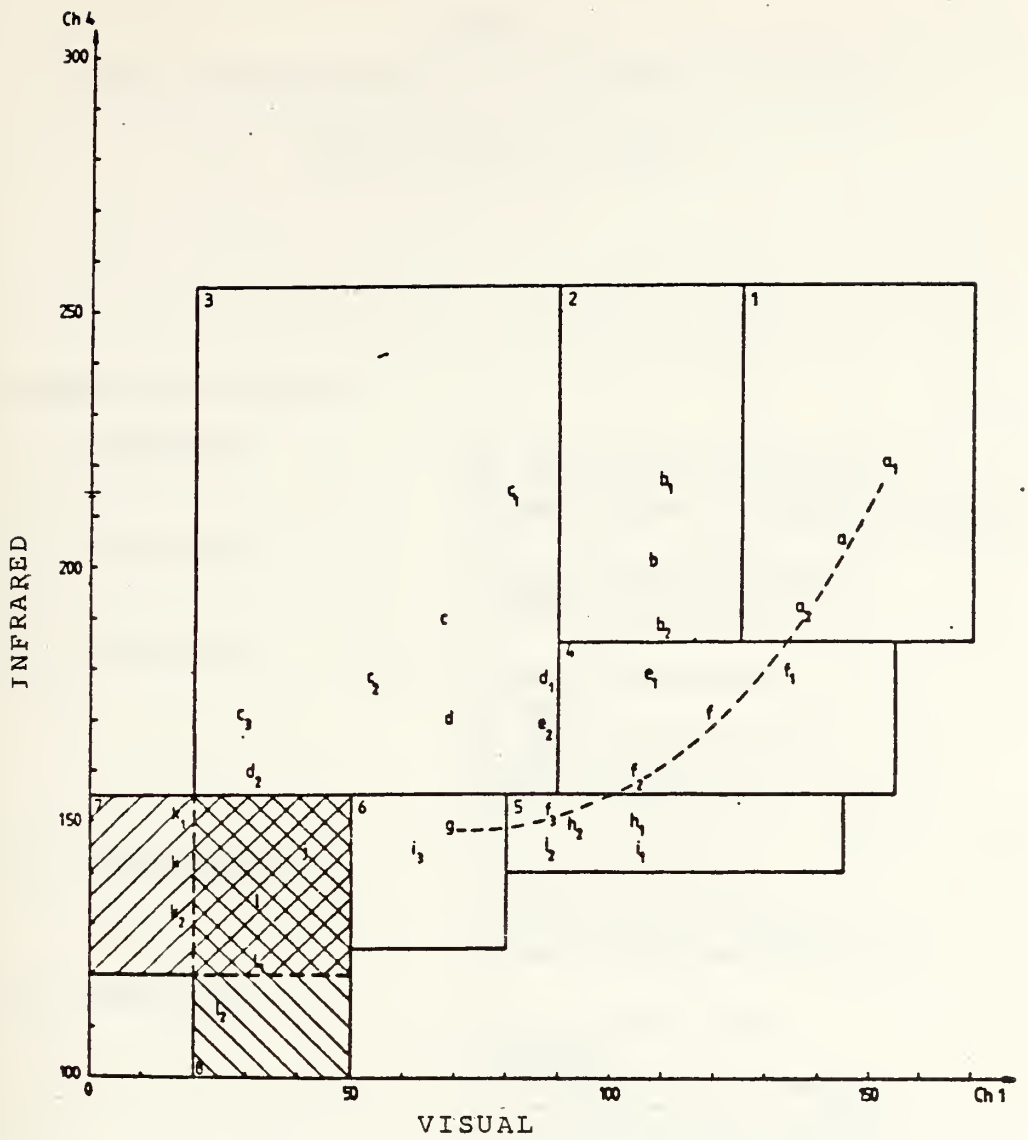

Figure 4. Two Dimension Decision Space for Typing Clouds from Visual and Infrared Digital Counts (Table II defines the symbols for the clouds) (from Liljas, 1981a)

August 1979 over a region encompassing Norway, Sweden, Finland, and the Baltic Sea with weather charts providing the ground truth. Based upon the precipitation threshold results of Muench and Keegan (1979), Liljas chose a cloud

TABLE II

Cloud Classification to be used with Fig. 4

(from Liljas, 1981a)

Main and Cloud Types:

1.	**Cumulonimbus**	**a**
		a_1 Storm cloud with high top
		a_2 Squall cloud with scattered showers
2.	**Nimbostratus**	**b**
		b_1 Large vertical thickness
		b_2 Rather low topside
3.	**Cirrostratus**	**c**
		c_1 Dense cirrostratus
		c_2 Cirrus
		c_3 Thin cirrus over water
		d_1 Dense altostratus
		d_2 Thin altostratus over water
		e_2 Thin altostratus
4.	**Cumulus congestus**	**f**
		e_1 Dense altocumulus
		f_1 Large piled up cumulus
		f_2 Rather small and flat cumulus
5.	**Stratocumulus**	**h**
		h_1 Dense stratocumulus
		h_2 Ordinary
		f_3 Slightly piled up cumulus with clear areas in between
		i_1 Very dense haze/stratus
		i_2 Dense haze/stratus
6.	**Haze/Stratus**	**i**
		i_3 Ordinary haze/stratus
		g Cumulis humilis
7.	**Land**	**l**
		j Haze over water
		l_1 Planting season spring or autumn
		l_2 Warm green season
8.	**Water**	**k**
		k_1 Cold
		k_2 Warm

top temperature threshold of -12°C to -15°C to classify cumulonimbus and nimbostratus clouds. Starting with this cloud classification and the assumption that the highest and densest clouds produce the maximum precipitation amount, Liljas suggested a qualitative precipitation intensity scale based on the sum of the visual and infrared satellite digital counts (see Table III). These sums represent the areas of the Liljas nimbostratus and cumulonimbus cloud types in his bi-spectral cloud classification (see Fig. 5).

TABLE III

Threshold Values Describing Precipitation Intensity Levels as Applied in Fig. 5 (from Liljas, 1981a)

	The Sum of Digital Levels	
Ch 1 + Ch 4	391-310	light rain
	311-330	
	331-350	
	351-370	
	371-390	
	390	very strong rain

Lovejoy and Austin (1979) studied rain mapping of cloud areas based on GOES visual and infrared satellite data over

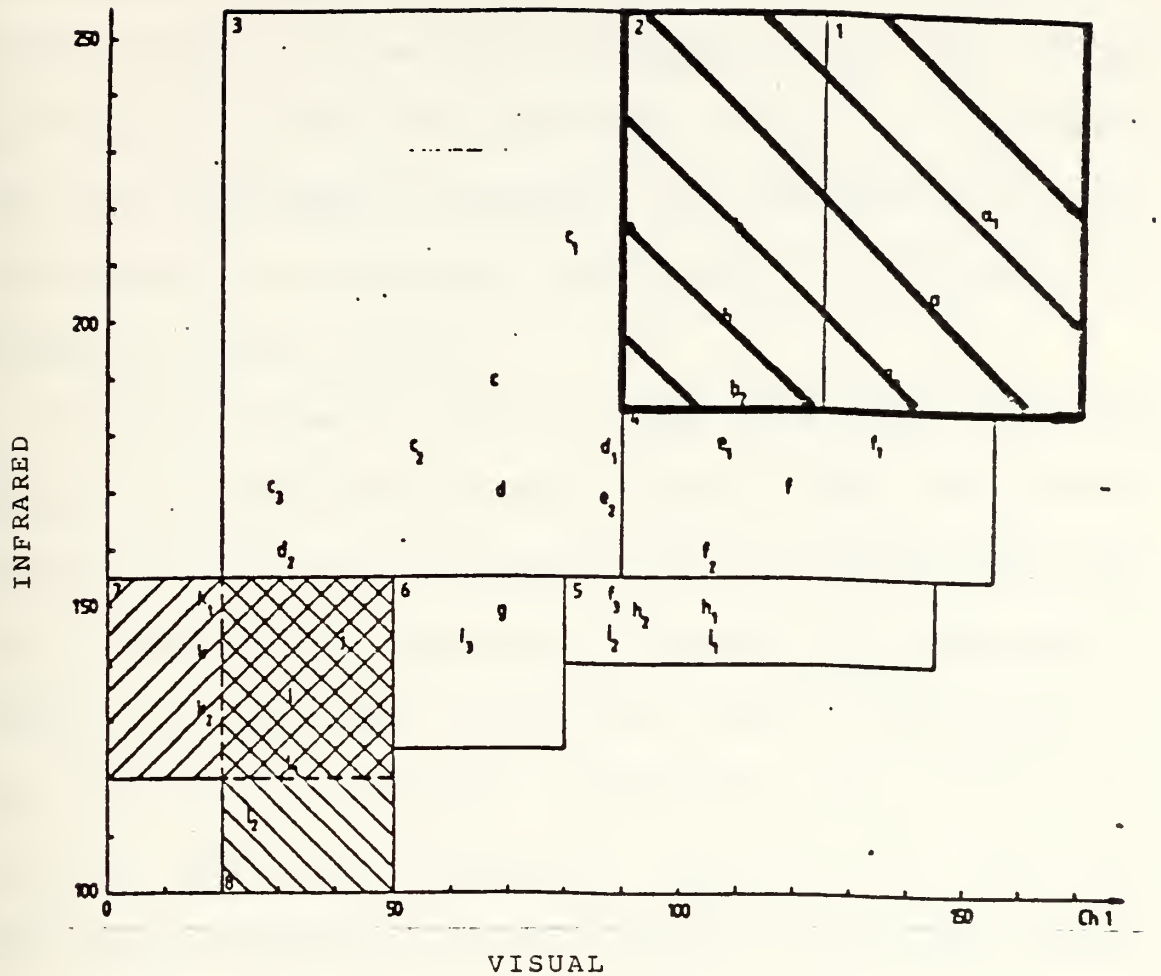

Figure 5. Precipitation Intensity Classification from Visual and Infrared Digital Counts. The Precipitation Area is Represented with the Dark Diagonal Lines. (See Table III for the mathematical description of the intensity areas.) (from Liljas, 1981a)

Montreal, Canada, and the tropical Atlantic (Global Atmospheric Research Program Atlantic Tropical Experiment, GATE, data) with radar data providing the ground truth. The Montreal data set consisted of 17 observations over three days

during June 1977. Working with 4 x 4 km resolution satellite image, Lovejoy and Austin plotted two dimensional frequency grids for the radar-determined rain and no-rain points on a 25 x 25 array (see Figs. 6 and 7). The visual data were normalized by selecting the "brightest" and "dimmest" values in each image and linearly interpolating the radiances between 0 and 1.

Lovejoy and Austin (1979) state, with reference to the cumulus rain data distribution of Fig. 6 that, "The distribution was to a good approximation a two-dimensional Gaussian." They do not describe or provide the statistics to support this assertion. The no-rain cumulus cases (Fig. 7) were described as a bimodal distribution with one peak near the low visual and low infrared values and the other peak near the rain peak but shifted slightly toward lower values. In most cases, the separation of the cumulus rain and no-rain cases was statistically significant with the probability ranging from 10% to 50% that the rain and no-rain samples came from the same population.

The Lovejoy and Austin (1979) two dimensional frequency plots for non-cumulus storms were limited to one case. The significant differences between the cumulus and non-cumulus

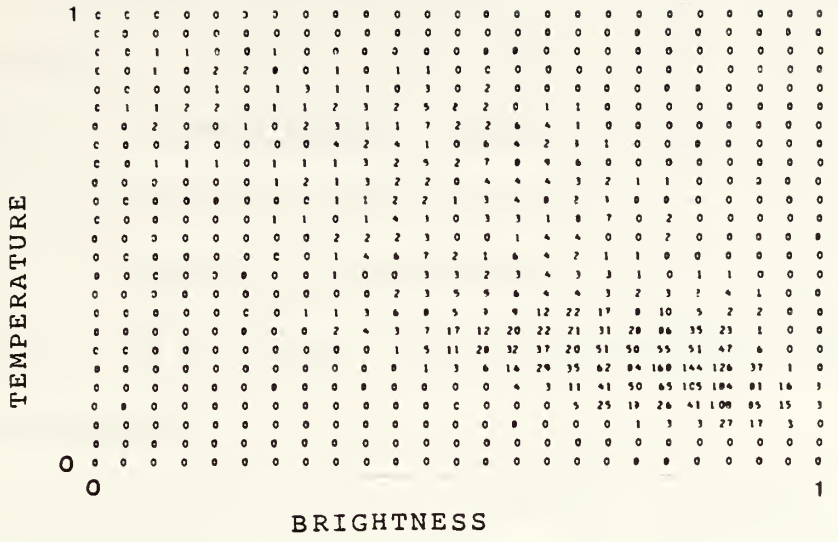

Figure 6. Frequency Plot of Rain Distribution for GATE day 248, 1300 GMT (from Lovejoy and Austin, 1979)

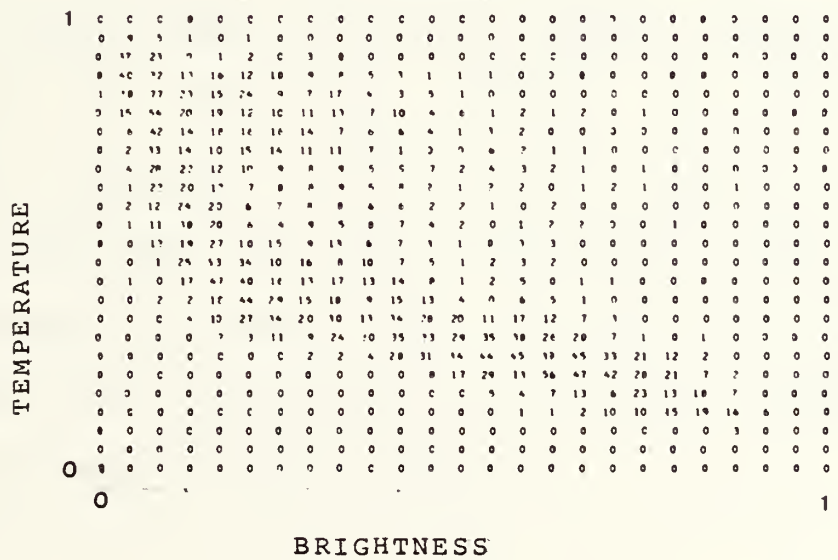

Figure 7. Frequency Plot of No-rain Distribution for GATE day 248, 1300 GMT (from Lovejoy and Austin, 1979)

data sets were that the non-cumulus no-rain plot lost its bimodal character, relative to the cumulus no-rain plot, and appeared as a broad two dimensional Gaussian distribution. The non-cumulus rain plot points fell within the no-rain distribution, but were shifted slightly higher in the visual. The separation of the non-cumulus rain and no-rain cases was not statistically significant, with greater than a 50% probability of the rain and no-rain samples coming from the same population.

Lovejoy and Austin (1979) attempted to further classify the cumulus rain and no-rain cases into no-rain, light rain, and heavy rain. Rainfall rates greater than 2 $mm\text{-}h^{-1}$, as determined by radar, were defined as heavy rain. As expected, the mean of the heavy rain cases was shifted slightly towards higher visual and infrared values than the mean of the light rain cases. However, the shift was so small that there was at least an 80% probability of the light rain and heavy rain cases coming from the same population. Lovejoy and Austin (1979) concluded that "little if any rainfall-rate information is contained in a single (visual and infrared) satellite image."

Lovejoy and Austin (1979) tested a spectral threshold technique for rain area mapping. Each satellite image of 400 x 400 km was divided into one hundred 40 x 40 km boxes. The 100 subareas were each checked with radar to determine the total number of rain areas. An equal total number of satellite subareas were classified as rain areas. The satellite subareas with the highest visual and highest (cold) infrared values were classified as rain areas, until the total number of satellite rain areas equaled the total number of radar determined rain areas. This spectral threshold technique was applied to three days accumulation of data and is shown in Tables IV and V. When compared with the success of the two dimensional frequency plot method, the visible and infrared thresholds averaged 45% and 58% worse, respectively. The accuracy of the visual threshold is limited by the extent of low, thick clouds and the infrared threshold is limited by the extent of the cirrus clouds in the satellite image. Lovejoy and Austin (1979) concluded that "the errors involved in using a 'best threshold' are very large indeed."

Del Beato (1981) studied correlations between cloud top temperatures (based on NOAA-5 satellite data) and rainfall

TABLE IV

Statistical Comparison of Rain Area Mapping Techniques

(R /R X 100 indicates "percentage of correct satellite rain")
(from Lovejoy and Austin, 1979)

Day	Opt. 2-D Boundary $(R_s/R) \times 100^a$	IR Optimum Threshold IR(K)	IR Optimum Threshold $(R_s/R) \times 100$	Visible Optimum Threshold (Scale: 0-1)	Visible Optimum Threshold $(R_s/R) \times 100$	Area Rain Coverage (%)	Total No. of Points
GATE							
242, 243, 246 247, 248, 251 252, 261	65	<232	53	>0.68	64	15.8	47706
Montreal							
152	56	<232	20	>0.88	31	9.7	40361
180	56	<247	55	>0.80	48	24.0	33738
153	53	<254	52	>0.88	49	15.9	22358

TABLE V

Statistical Comparison of the Accuracy of Rain Areas

(from Lovejoy and Austin, 1979)

Technique	Region	Number of Images or Sequences	Bias	Error Factor	E_{RMS}
2-D Pattern Matching	Montreal	17	1.13	1.26	0.22
2-D Pattern Matching	Montreal	3	1.08	1.19	0.18
Optimum IR Threshold	Montreal	3	1.38	1.74	0.71
Optimum Visible Threshold	Montreal	3	1.54	1.59	0.58
2-D Pattern Matching	GATE	8	1.21	1.41	0.25

totals for 30- and 60-min intervals over eastern Australia. The satellite data had a 60 km² maximum resolution at subsatellite point and cloud top temperatures were area averaged for a resolution of 200 km². The 21 data sets were first classified according to synoptic situation in a rough

attempt to group the data by cloud type, droplet spectra, and air mass trajectory. The initial results suggested that the cloud top temperature determined an upper limit on rainfall amount, with the maximum increasing as the cloud top temperature decreases. A linear correlation analysis to determine a quantitative relationship between rainfall amount and cloud top temperature gave indefinite results.

Further study of surface and radiosonde observations indicated that classification by proportion of cumuliform cloud reports to all cloud reports and subcloud layer humidity might be more appropriate (Del Beato, 1981). This classification resulted in a correlation coefficient of 0.90, excluding cases with cumuliform portions less than 50% and dew-point depressions of greater than 6°C. Finally, a composite frequency distribution was calculated based on three cases, all southwesterly stream situations described as "post-frontal cellular convection cases in cyclonically curved flow." The fitted equation was:

$$f = 0.057 - 0.004CTT - 0.054R \qquad (1)$$

where f is the rainfall frequency, R is the 30-min rain total (mm), and CTT is the cloud top temperature (°C). The

equation was fitted to 41 independent f values. This equation is associated with a correlation coefficient of 0.79 at the 99% confidence level. Equation (1) indicates no rain from clouds warmer than +13°C and a maximum 30-min rainfall of 2.5 mm for a cloud top temperature of -20°C.

In summary, Del Beato (1981) found that cloud top temperatures and 30- and 60-min rainfall totals indicated statistically significant relationships for cloud systems with a high proportion of cumulus clouds and high subcloud humidity. Additionally, as cloud top temperatures decrease to at least -35°C, rainfall totals increase.

Wylie (1982) attempted to correlate rainfall occurrence with radiosonde soundings, hourly Service-A observations, and visual and infrared satellite data. His data sample was restricted to "large-scale cloud cover" areas with widespread precipitation (rain gauge reports varied less than 20%) for the Great Plains States region for the period 27 February 1981 through 4 January 1982. From thirteen parameters derived from the three data sources (see Table VI), the best linear regression equation for estimating rainfall rates was:

$$\text{6-hour rain (in)} = 1.0242 + 0.380Pw - 0.0304Qc - 0.0047Ct \qquad (2)$$

where Pw is the vertically integrated precipitable water vapor (in), Qc is the moisture convergence (g/kg/day), and Ct is the cloud top temperature (Kelvins). Equation (2) has a linear correlation coefficient of 0.60. Linear regression equations were also determined for the three parameters alone and for a combination of Pw and Qc to be used when not all three data types were available. The cloud temperature regression equation was:

$$6 \text{ hour rain (in)} = 2.10 - 0.008Ct \qquad (3)$$

The correlation coefficient was -0.35. Wylie (1982) stated that the synoptic scale data base measurements were best suited for estimating broad changes in rainfall rates associated with changes in air masses and not suited for estimating rainfall rates associated with small scale dynamic processes.

C. LIFE HISTORY

The life history methods are empirically derived precipitation estimation schemes based upon two assumptions, first, that significant rainfall comes from convective clouds, and second, that convective clouds can be identified and measured in satellite images. These methods involve manual analyses of convective cloud areas in a sequence of

TABLE VI

Correlation Coefficients for Determination of Precipitation Based on the Three Data Types (from Wylie, 1982)

MEASURED PARAMETER	CORRELATION WITH 6 HOUR PRECIP. REPORT	NUMBER OF CASES	F
Vertically integrated precipitable water vapor	0.48	196	58*
Cloud top brightness	-0.44	184	44*
Cloud top height	-0.40	190	36*
Moisture convergence	0.38	184	31*
Cloud top temperature	-0.35	199	27*
Bubble model predicted cond.	0.27	115	9
500 mb vorticity advection	-0.21	173	8*
Parcel lifted index	-0.20	200	8*
700 mb temperature advection	0.20	173	7*
Sfc temperature advection	0.19	156	6
850 mb temperature advection	0.17	189	6
Wind convergence (sfc)	0.09	167	1
Vertical wind shear	0.03	156	0

* Significant correlation at the 99% level.

visual, infrared, or both visual and infrared satellite images. Threshold values and study condition parameters

associated with published life history studies are summarized in Table VII.

TABLE VII

Summary of Life History Threshold Values

STUDY	LOCATION	CASES	TIME OF YEAR	THRESHOLD VALUE INFRARED	VISUAL
Griffith, et al., (1978)	Florida, Venezuela, Honduras, and hurricanes impacting East Coast United States	34 days	summers 1969-1976	-20°C	80 counts*
Stout, et al., (1979)	tropical North Atlantic	57 observations	September 1974	-26°C	0.45 albedo (sun overhead)
Wylie (1979)	Montreal	6 days	June 1977 September 1977	-16°C	-
Negri and Adler (1981)	Oklahoma, Arkansas, Missouri	1 day (15 thunderstorms)	April 24, 1975	-27°C	-

* ATS-3 satellite

The Scofield/Oliver (Scofield, 1981) analysis follows a decision tree procedure to estimate half-hourly rainfall for deep convective systems within tropical air masses. Using enhanced infrared and high resolution visual satellite

images, the technique involves first identifying the active convective portion of the cloud, or cluster, from two consecutive satellite images. Once the active portion is identified, the half-hourly rainfall estimation is computed based on such factors as cloud top temperature, cloud growth, and departure of precipitable water from a summertime normal.

The Griffith/Woodley (Griffith et al., 1978) technique is designed to estimate rainfall in the tropics, over large space and time scales, using geosynchronous visual or infrared satellite imagery. This time-dependent technique was empirically derived as a relationship between cloud area, echo area, and rain rate for two areas in south Florida, with raingage-radar providing the ground truth, and was then tested in other tropical areas. This scheme was subsequently tested further in extratropical areas (Griffith et al., 1980), with modifications to the rainfall amount predicted.

The determination of a cloud area-rainfall relationship first required the specification of both a visual and an infrared threshold to define the cloud area. The visual brightness threshold, normalized for radiation geometry, was

80 counts for the third Application Technology Satellite (ATS-3) and the infrared threshold was 253K (-20°C). The thresholds were based on a comparison of the clouds with a given maximum digital count and the radar echoes associated with these clouds.

The empirical cloud area-rainfall relationship was derived as a two step process. First, a relationship between the cloud area and the radar echo area, normalized for the maximum area achieved by the cloud or cluster, was established for the visible and infrared satellite data. Second, the relationship between the echo area and rain volume was determined and was of the form:

$$Rv = I\ Ae \qquad (5)$$

where Rv is rain volume per hour (m^3-h^{-1}), I is rain in units of (m^3-km^{-2}-h^{-1}), and Ae is the echo area (km^2) defined by the 1 mm-h^{-1} rain rate. Thus, given a time sequence of convective clouds (or cluster areas) measured from visible or infrared satellite images, volumetric rain rate can be estimated.

Stout *et al.* (1979) modified the Griffith/Woodley technique (Griffith *et al.*, 1978) to estimate volumetric rain

rate directly from a cumulonimbus cloud area and area change according to the equation:

$$R = a_0 A + a_1 dA/dt \qquad (6)$$

where R is the volumetric rainfall of the cloud (m^3-s^{-1}), A is the cloud area (m^2), dA/dt is the change of cloud area over time (m^2-s^{-1}), and a_0 and a_1 are constants with dimensions m-s^{-1} and m, respectively. The two constants were calculated by a least squares fit of cloud area-rain rate pairs based on visible and infrared geosynchronous satellite data and 5.3 cm ship radar rain data collected during GATE. The cloud area and its change are defined by the threshold value. The visible threshold for cloud area calculations was 60 digital counts on the ATS-3 (corresponding to an albedo of 0.45 with the sun overhead), or equivalently 172 digital counts on the first Geosynchronous Meteorological Satellite (SMS 1). The infrared threshold was 160 digital counts (-26°C). The standard error between the estimated rainfall and the mean radar rainfall was 62% and 76% for the visual and infrared equations respectively.

Wylie (1979) attempted to use the tropical convective rainfall techniques of Griffith et al., (1978) and Stout et

al., (1979) for estimating precipitation in Montreal, Canada. Using visual satellite data, corrected for the changing sun angle (Mosher, 1975), infrared satellite data, and 10.0 cm radar meaured rainfall rates, Wylie studied six days of precipitation, three days each in June and September 1977. Wylie concluded that because of air mass differences between Montreal and the tropics, the Griffith and Stout estimation techniques did poorly in Montreal, Canada. The singlemost important limitation with these two schemes was the difficulty of measuring cumulonimbus cloud area when the "anvils were often merged into large cloud masses and the extensive stratus cloud cover often obscured the pictures." Wylie also noted that the Griffith et. al. (1978) threshold of -26°C had to be changed to -16°C for the summertime Montreal, Canada, area. With the warmer cloud top temperatures the cloud areas were a larger, more appropriate size for tracking.

Wylie (1979) then attempted to combine sounding data input into a one-dimensional model (Simpson and Wiggert, 1969) and satellite cloud cover measurements to estimate rainfall for Montreal. With the GATE measurements for rain rates associated with satellite-derived cloud areas and the

model output, rainfall rates were estimated by multiplying the two values. The most accurate estimations were for the cumulus clouds in the warm air masses occurring in June, the cases the model was designed to handle. Wylie concluded that in order to estimate rainfall in all geographical areas and seasons a more sophisticated model would be needed.

Negri and Adler (1981) did one case study of fifteen thunderstorms in the Oklahoma, Arkansas, and Missouri area on 24 April 1975. They used radar data for ground truth and had special 5 minute GOES-E satellite passes over the area of interest. They were able to determine that the precipitation began falling, as indicated by radar data, for cloud top temperatures ranging from 229K to 260K (-44°C to -13°C). The mean cloud top temperature value was 247K (-26°C).

III. DATA PROCESSING

A. INTRODUCTION

The data set assembled for this study consists of collocated GOES-E satellite data and Service-A hourly surface observations for the southeastern United States during August 1979. The GOES-E data consists of 10 x 10 pixel matrices of visual and infrared satellite data centered over each of 137 surface stations (Fig. 8) all south of 40°N. The satellite data are measured with the Visual Infrared Spin Scanned Radiometer (VISSR) which have subsatellite point spatial resolutions of 1 and 7 km for the visual and infrared channels, respectively. The GOES-E navigation was completed by Man-computer Interactive Data Access System (McIDAS) at the University of Wisconsin using the full resolution visual data, with an accuracy of 1-2 pixels (1-2 km). The full resolution visual data were averaged to a 7 km resolution, to equal the infrared data resolution. The visual and infrared digital counts range from values of 0-255. The 10 x 10 pixel GOES-E visual and infrared satellite data each cover an area 45 nmi x 45 nmi at 30°N (60 nmi x 60 nmi at

42°N). The Service-A hourly reports total 70,623 observations. No Service-A specials or record-specials are included.

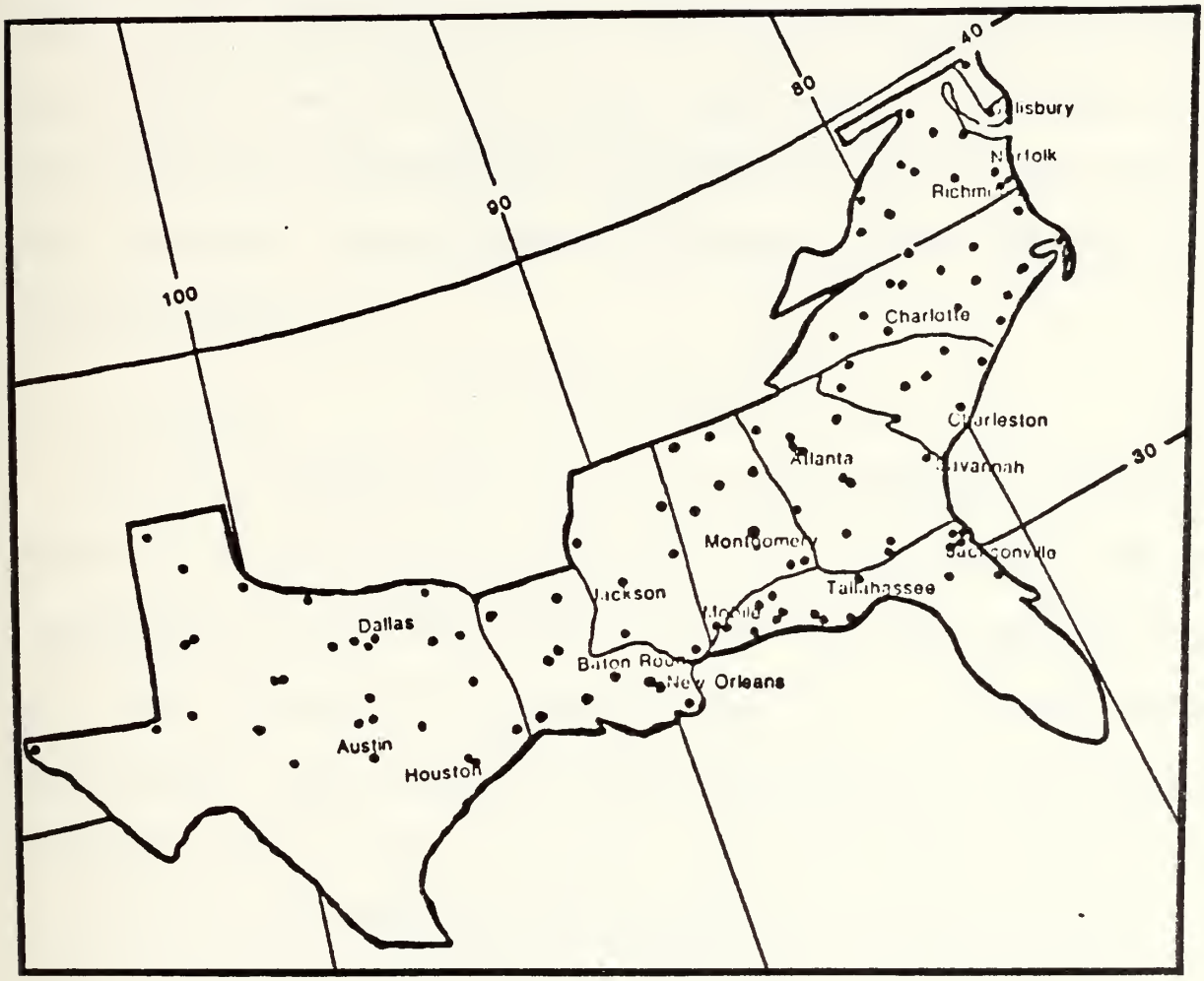

Figure 8. Geographical Locations of Service-A Station Report Data

The data are divided into two no-precipitation categories (Table VIII) and seven precipitation categories (Table

IX) to investigate precipitation specification, convective versus continuous precipitation specification, and qualitative specification of light versus moderate/heavy precipitation. The pixel array size is also varied from the 10 x 10 array size to an 8 x 8, a 6 x 6, and a 4 x 4 array size to investigate the differences in the data resulting from various resolution sizes within a particular weather condition classification.

B. DATA SORT

For the combined visual and infrared threshold specification of precipitation, satellite data for 1200-2000 GMT, corresponding to 0800-1600 EDT, were sorted into precipitation and no-precipitation groups (Fig. 9). The 0800-1600 EDT interval was chosen to avoid distortion of the visual satellite data due to a low solar elevation angle. The visual data were normalized and converted to albedos based on the work done by Muench and Keegan (1979). This scheme corrects for the varying zenith angle as well as adjusting the visual satellite data for anisotropic scattering as related to the zenith angle. (See Appendix A for further specific information concerning the Muench and Keegan normalization scheme.)

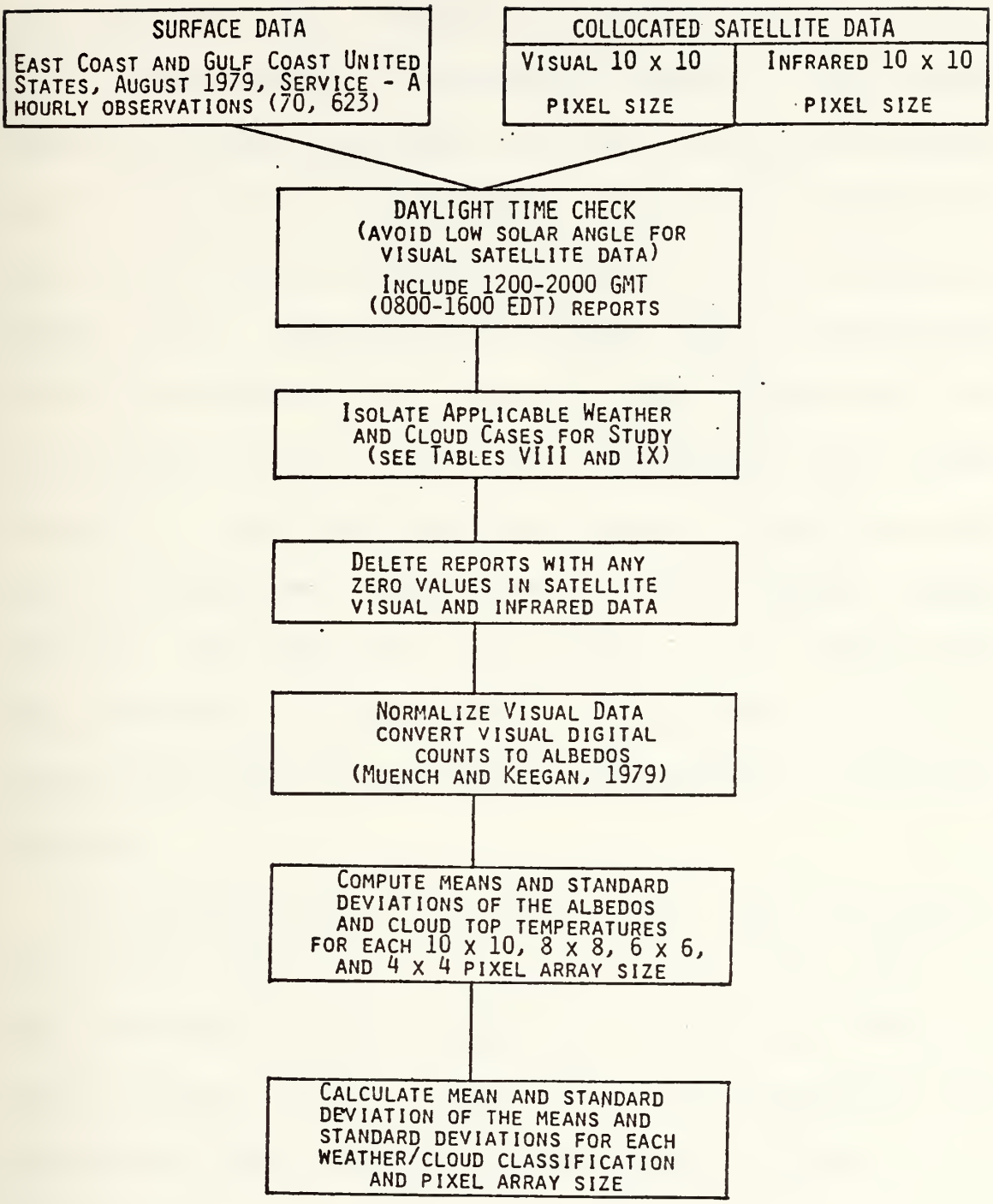

Figure 9. Flow Chart of Data Processing

While albedo values cannot exceed 1.00, the Muench and Keegan (1979) scheme allows the values to overshoot 1.00, up to a value of 1.20. Therefore, the visual satellite values are not true albedos, but estimated albedos. The extended visual normalized data scale was used to facilitate comparison of the results in this effort to the most extensive bispectral threshold precipitation specification of Muench and Keegan (1979). The Muench and Keegan (1979) normalization scheme specifies that any computed albedo greater than 1.20 be set equal to 1.20 to limit the unreasonably large values. Similiarly, the scheme specifies computed albedos less than 0.15 be interpreted as the ground or water surface reflectance and the value 0.00 be assigned. The infrared data were processed in digital counts and converted to cloud top temperatures prior to statistical computations and graphical displays.

The no-precipitation data (Table VIII) are comprised of the digital visual and infrared 10 x 10 pixel arrays of those Service-A station reports not showing any "R" in the current weather group. Thus, the no-precipitation group includes stations reporting drizzle (weather codes L-, L, and L+).

TABLE VIII

Classification of Nc-Precipitation Data Groups

Category	Name	Service-A Current Weather/ Cloud Group	Reports
2A	No-Precipitation, Overcast Ceiling	no "R"/ Cloud Groups 300, 030, 003, 130, 230, 013, 023, 103, 203, 113, 123, 213, 223	1976
2B	No-Precipitation, Overcast and Broken	no "R"/ Cloud Groups (above groups) and 200, 020, 120, 220, 002, 102, 202, 112, 122, 212, 222	7358

The no-precipitation data are divided into two categories, overcast ceiling (category 2A) and overcast and broken ceiling (category 2B). Cloud cover is based on the three digit cloud group in the Service-A surface observation. The first digit indicates the amount of low clouds, where 0 is defined as clear, 1 is scattered (one-eighth to four-eighths cloud cover), 2 is broken (five-eighths to seven-eighths cloud cover), and 3 is overcast (eight-eighths cloud cover). The second and third digit indicate the amount of middle and high clouds, respectively. The same 0-3 values defined for the low clouds are used for middle and high cloud amount.

The precipitation data (Table IX) are comprised of the visual and infrared 10 x 10 pixel arrays of those Service-A station reports showing any "R" in the current weather group. Two precipitation observations were excluded from the data set because each report also indicated clear skies.

TABLE IX

Classification of Precipitation Data Groups

Category	Name	Service-A Current Weather	Reports
1	Precipitation	any "R"	538
1A	Precipitation Overcast Ceiling	any "R" and overcast ceiling (as defined in Table VIII category 2A)	329
1B	Precipitation Overcast and Broken Ceiling	any "R" and overcast and broken ceiling (as defined in Table VIII category 2B)	534
1C	Continuous Precipitation	R-, R, R+	112
1D	Convective Precipitation	RW-, RW, RW+, TRW-, TRW, TRW+, TR-, TR, TR	426
1E	Light Precipitation	R-, RW-, TRW-, TR-	464
1F	Moderate/Heavy Precipitation	R, R+, RW, RW+, TRW, TRW+, TR, TR	74

The general precipitation data (category 1) are divided into six groups: precipitation overcast ceiling (category

1A), precipitation overcast and broken ceiling (category 1B), continuous (category 1C), convective (category 1D), light (category 1E), and moderate/heavy (category 1F) precipitation. These seven precipitation groups are used to investigate precipitation specification, convective versus continuous precipitation specification, and qualitative specification of light versus moderate/heavy precipitation.

C. STATISTICAL TREATMENT

The means and standard deviations of albedos and cloud top temperatures of each 10 x 10 pixel array for the weather types listed in Tables VIII and IX were calculated. Means and standard deviations of albedos and cloud top temperatures were also calculated for the 8 x 8, 6 x 6, and 4 x 4 pixel arrays centered over the surface station. The 8 x 8, 6 x 6, and 4 x 4 pixel arrays are equal to 36 nmi x 36 nmi, 27 nmi x 27 nmi, and 22 nmi x 22 nmi at 30°N respectively. Variation of the digital satellite areal coverage is used to investigate the differences in the statistics due to the chosen resolution size.

The data sets in Tables VIII and IX are represented, first, by the mean and standard deviation of the resolution cell means and standard deviations. Second, these data sets

are represented by the distributions of the mean cloud top temperatures and albedos where the mean cloud top temperatures are sorted into ten Kelvin (K) intervals and the mean albedos are sorted into 0.10 intervals. These representative statistics and distributions are calculated for the four pixel array sizes.

The statistical and distribution results for differing resolution sizes, bi-spectral threshold specification of precipitation, and separation of light from moderate/heavy precipitation are discussed in Chapter IV.

IV. RESULTS

A. INTRODUCTION

The figures presented in this chapter display the distributions of the grand means of the resolution cell means of albedos and cloud top temperatures for the data sets listed in Tables VIII and IX for the four array sizes. The mean values are sorted into ten Kelvin intervals and 0.10 estimated albedo intervals.

B. RESOLUTION

The effect of satellite resolution in representing general precipitation (category 1) and no-precipitation overcast (category 2A) data are explored for four resolution sizes. The four sizes are 10 x 10, 8 x 8, 6 x 6, and 4 x 4 and are approximately equal to areas of 2025 nmi^2, 1296 nmi^2, 729 nmi^2, and 484 nmi^2 at 30°N respectively.

The general precipitation (category 1) and no-precipitation overcast (category 2A) data were chosen for study because, while they represent two different weather conditions, their albedo and cloud top temperature distributions have the largest amount of overlap when compared to any

other pair of precipitation versus no-precipitation data sets. The possibility arises that statistical differences in the four resolution sizes might be sufficient or complement other information in delineating these two weather conditions.

1. Precipitation Data

The general precipitation (category 1) data are comprised of 329 overcast ceiling reports (61%), 205 broken ceiling reports (38%), and 4 scattered ceiling reports (1%).

a. Mean Statistics

The precipitation data (category 1) differences between the means of the cell means visual and infrared 10 x 10 and 4 x 4 array sizes are 0.035 and 2.2K, respectively (Table X). The trend of the mean of the means is toward higher albedo values and colder cloud top temperatures with the decreasing area or array size. The standard deviations of the means similiarly show an increase in the albedo, 0.016, and cloud top temperature, 1.0K, from the 10 x 10 array size to the 4 x 4 array size.

b. Standard Deviation Statistics

The standard deviation statistics display the opposite trend with decreasing area as the mean statistics.

TABLE X

Precipitation Data Statistics for Four Array Sizes

Overcast, Broken, and Scattered Ceilings

		10 x 10	8 x 8	6 x 6	4 x 4
Mean of Means	(VIS)	.579	.591	.603	.614
	(IR)	253.0K (-20°C)	252.2K (-21°C)	251.4K (-22°C)	250.8K (-22°C)
Standard Deviations of Means	(VIS)	.211	.214	.219	.227
	(IR)	20.7K	21.0K	21.3K	21.7K
Mean of Standard Deviations	(VIS)	.173	.161	.144	.124
	(IR)	10.4K	9.1K	7.6K	5.6K
Standard Deviation of the Standard Deviations	(VIS)	.078	.078	.075	.072
	(IR)	7.0K	6.7K	6.0K	4.9K

The means and standard deviations of the standard deviations decrease in the visual and infrared values with decreasing area (Table X). The differences between the 10 x 10 and 4 x 4 array sizes visual and infrared means of the standard deviations are 0.049 and 4.8K, respectively, and the standard deviations of the standard deviations are 0.006 and 2.1K, respectively.

c. Distribution Discussion

The distributions of the precipitation data are shown in Figs. 10, 11, 12, and 13. There is a discernible shift toward higher albedos and colder cloud top temperatures of the 2% and 3% frequency isopleth with decreasing array size. This upward shift is also reflected in the mean of the means (Table X). The appearance of the 5% frequency isopleth in the 6 x 6 and 4 x 4 array sizes at high albedos and cold cloud top temperatures highlights the shift.

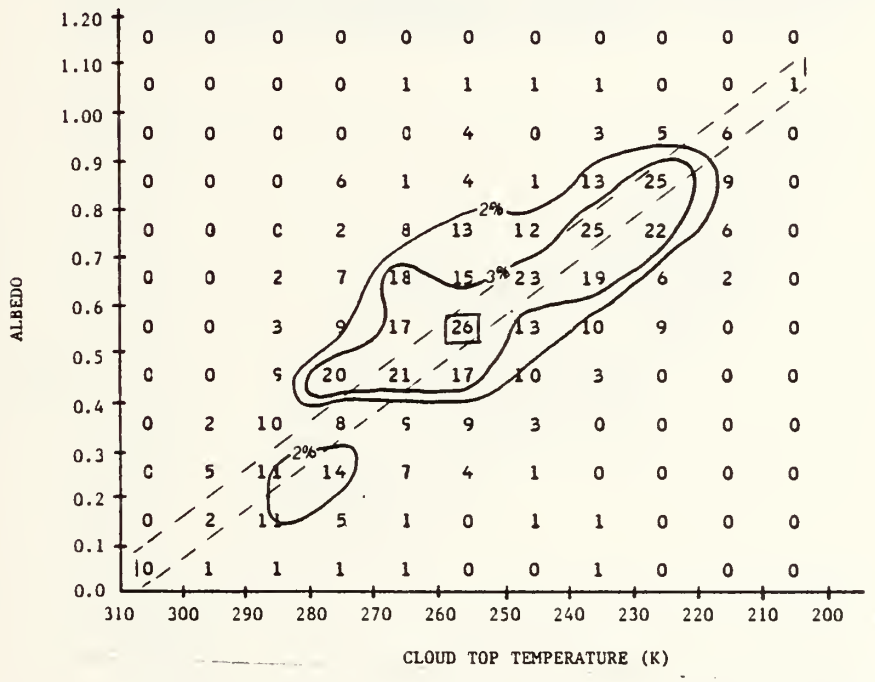

Figure 10. Precipitation Data for 10 x 10 Array Size (The mean, .579 and 253.0K, interval is boxed. The 2% and 3% frequencies are for 11 and 16 occurrences, respectively.)

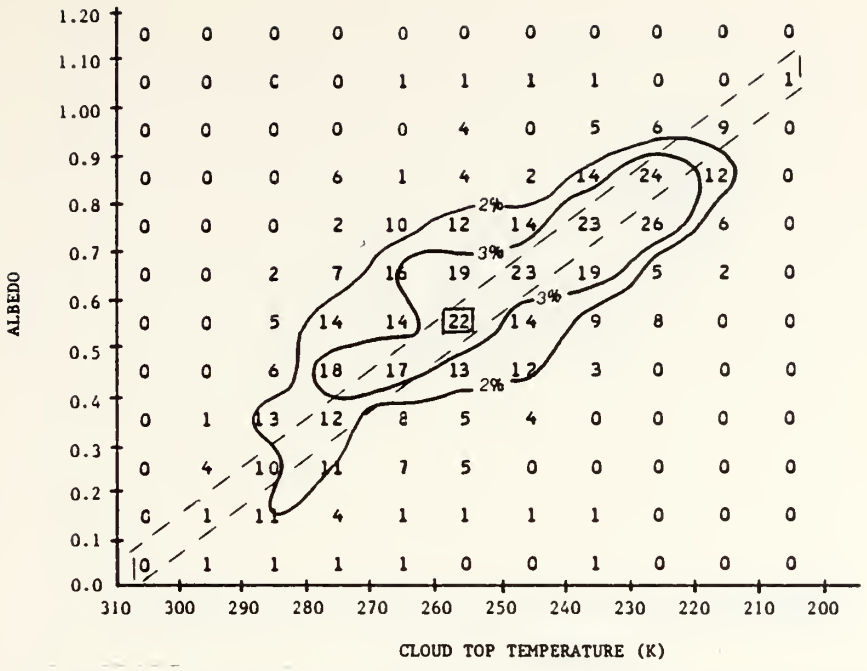

Figure 11. Precipitation Data for 8 x 8 Array Size (The mean, .591 and 252.2K, interval is boxed. The 2% and 3% frequencies are for 11 and 16 occurrences, respectively.)

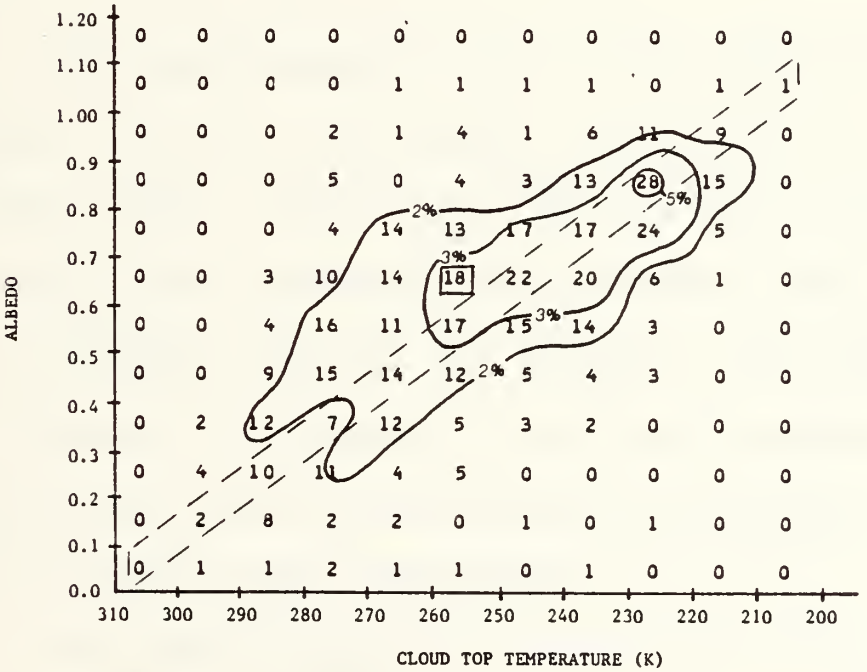

Figure 12. Precipitation Data for 6 x 6 Array Size (The mean, .603 and 251.4K, interval is boxed. The 2%, 3%, and 5% frequencies are for 11, 16, and 27 occurrences, respectively.)

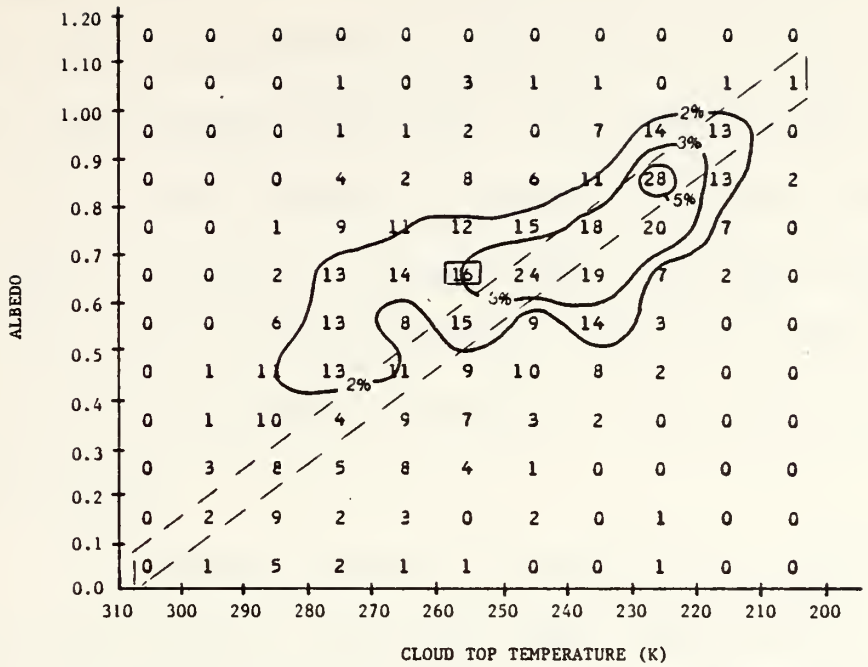

Figure 13. Precipitation Data for 4 x 4 Array Size (The mean, .614 and 250.8K, interval is boxed. The 2%, 3%, and 5% frequencies are for 11, 16, and 27 occurrences, respectively.)

The distributions of the 10 x 10 and 8 x 8 array sizes (Figs. 10 and 11) are unimodal while the 6 x 6 and 4 x 4 array sizes (Figs. 12 and 13) appear to be more bimodal. The four array sizes were tested for a Gaussian distribution with the Chi-square test and all failed at any confidence level. Therefore, differences in the four resolutions cannot be adequately tested by well defined statistical methods based on an assumed normal distribution.

The similiarities between the 10 x 10 and 8 x 8 array sizes (Figs. 10 and 11) and the 6 x 6 and 4 x 4 array

sizes (Figs. 12 and 13) are further illustrated in Fig. 14. A diagonal cut is plotted for each of the four array sizes where the lines plotted are shown as a dashed boxed area in Figs. 10-13. The diagonal cut reveals the close agreement between the 6 x 6 and 4 x 4 array sizes along the line. The 10 x 10 and 8 x 8 array size lines follow the same general trend but do not coincide as closely as the 6 x 6 and 4 x 4 array size lines.

The chosen diagonal line results in the 8 x 8 array size distribution appearing more smoothed than the 10 x 10 (Fig. 14), as there is no relative minima at the 4.0 interval for the 8 x 8 array size. The 10 x 10 array size, with the greater areal extent and therefore more averaging of differing clouds and clear areas, is expected to possess the "smoothest" appearance, the lowest number of relative maxima and minima of the four array sizes. However, the 8 x 8 array size actually displays the fewest relative maxima and minima along the chosen diagonal line. The smoother 8 x 8 array size cannot be explained in terms of significant differences in the number of cases of different ceiling types or different precipitation types occurring in interval 4.0 between the four array sizes. Quite simply, the

smoother 8 x 8 array size apparently results from the sorting intervals chosen for the distributions.

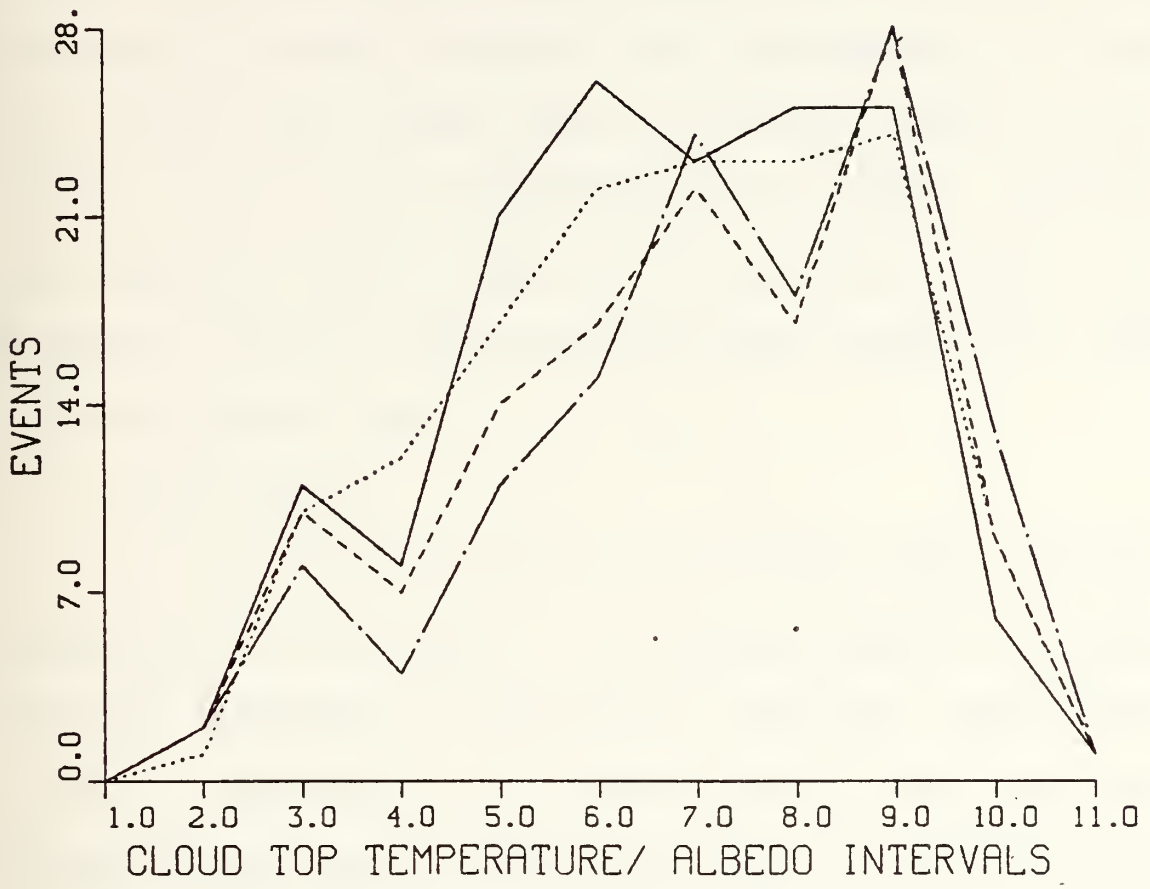

Figure 14. Precipitation Array Size Distributions Along Diagonal Line (The line represents the 10 x 10, dotted line the 8 x 8, dashed line the 6 x 6, and dash dot line the 4 x 4 array size.)

The elongated shape of all four precipitation distribution array sizes (Figs. 10, 11, 12, and 13) reveal the variation in the areal amount of cloudiness and precipitation. The distributions range from high albedos and cold cloud top temperatures (indicative of satellite fields of

view filled with precipitating clouds) to low albedos and warm cloud top temperatures (indicative of satellite fields of view partially filled with precipitating clouds). The visual and infrared satellite data distributions in Figs. 10, 11, 12, and 13 agree with the elongated shapes of Platt (1981) for his cloud classifications of cumulus, frontal, and jetstream cirrus clouds and agree with Coakley and Bretherton (1982) for their general clouds present in a 1000 km^2 Pacific Ocean area.

d. Summary

A satellite field of view filled with a precipitating cloud is expected to have higher albedo and colder cloud top temperature values than a partially filled field of view. Additionally, the filled field of view would have a more uniform texture, as reflected in variance or standard deviation values, than a partially filled field of view. The statistics discussed in this study confirm these expectations for this data set. As the array size or field of view is decreased, the mean statistics increase while the standard deviation statistics decrease (Table X).

For the precipitation data (category 1), there are significant differences between the four resolution

sizes. These differences are reflected in the upward trend in albedos and colder cloud top temperatures of the mean and the standard deviation of the means with decreasing area or array size (Table X). The reverse trend is found in the mean and standard deviation of the standard deviations.

The distributions have significant differences also. The relatively coarse resolution 10 x 10 and 8 x 8 array sizes have a unimodal distribution while the relatively fine resolution 6 x 6 and 4 x 4 have a bimodal distribution.

The four array sizes discussed vary in their statistics and distributions in representing the precipitation (category 1) data. The choice of satellite resolution for representation of the precipitation data will influence comparison of these data with other data. Therefore, for the remainder of this study the precipitation data for all classifications will be discussed using both the 10 x 10 and 4 x 4 array size.

One additional topic to explore is that a number of cases with albedos less than 0.40 appear in the precipitation data (category 1) in all four size distributions (Figs. 10, 11, 12, and 13). These low albedo values suggest

the possibility that there might be a consistent low bias in the normalization scheme. But a closer look at the individual reports with albedos less than 0.40 show no pattern involved with either the GMT hour or the longitude or latitude of these station reports. Further analysis of these low albedo precipitation reports are discussed in the light precipitation section (IV.E.).

2. No-precipitation Overcast Data

a. Mean Statistics

For the no-precipitation overcast cases (category 2A), differences between the means of the means visual and infrared 10 x 10 and 4 x 4 array sizes are 0.011 and 0.3 K, respectively (Table XI). The 0.3K infrared difference is within the 0.5K noise level of the VISSR infrared sensor. The trend of the visual mean of the means is upward with the decreasing array size. The standard deviations of the means show an increase in the albedo, 0.014, and cloud top temperature, 0.8K, from the 10 x 10 to 4 x 4 array sizes. Once again, both mean statistics have an upward trend with decreasing array size.

TABLE XI

No-Precipitation Data Statistics for Four Array Sizes

Overcast Ceiling

		10 x 10	8 x 8	6 x 6	4 x 4
Mean of Means	(VIS)	.407	.411	.415	.418
	(IR)	272.6K (-1°C)	272.5K (-1°C)	272.4K (-1°C)	272.3K (-1°C)
Standard Deviations of Means	(VIS)	.205	.208	.213	.219
	(IR)	17.8K	18.1K	18.3K	18.6K
Mean of Standard Deviations	(VIS)	.122	.113	.102	.087
	(IR)	5.4K	4.7K	3.9K	2.9K
Standard Deviation of the Standard Deviations	(VIS)	.056	.054	.052	.049
	(IR)	4.8K	4.4K	3.9K	3.1K

b. Standard Deviation Statistics

Conversely, the standard deviation statistics have a downward trend with decreasing area size. The differences between the 10 x 10 and 4 x 4 array visual and infrared means of the standard deviations are 0.035 and 2.5K, respectively. The differences in the standard deviations of the standard deviations are 0.007 in the visual and 1.7K in the infrared values.

c. Distribution Discussion

The distributions of the no-precipitation overcast data are shown in Figs. 15, 16, 17, and 18. These distributions are quite different from the precipitation distributions (Figs. 10, 11, 12, and 13). As expected, the no-precipitation overcast data are clustered at the low albedo and warm cloud top temperature values. The 5% frequency isopleths in Figs. 15, 16, and 17 show a grouping of the data at albedos ranging from 0.30 to 0.50 and cloud top temperatures from 280K to 290K. A bimodal distribution appears in the finer resolution 8 x 8, 6 x 6, and 4 x 4 array sizes (Figs. 16, 17, and 18). This shifting of the no-precipitation overcast data into two relative maxima for the three smallest array sizes is the sole significant difference in the four distributions.

d. Summary

The no-precipitation overcast data display an upward trend in the two mean statistics with decreasing array size, although the 0.3K mean of the means infrared difference is not significant. Conversely the two standard deviation statistics decrease with decreasing array size. These trends are consistent with the expected statistical

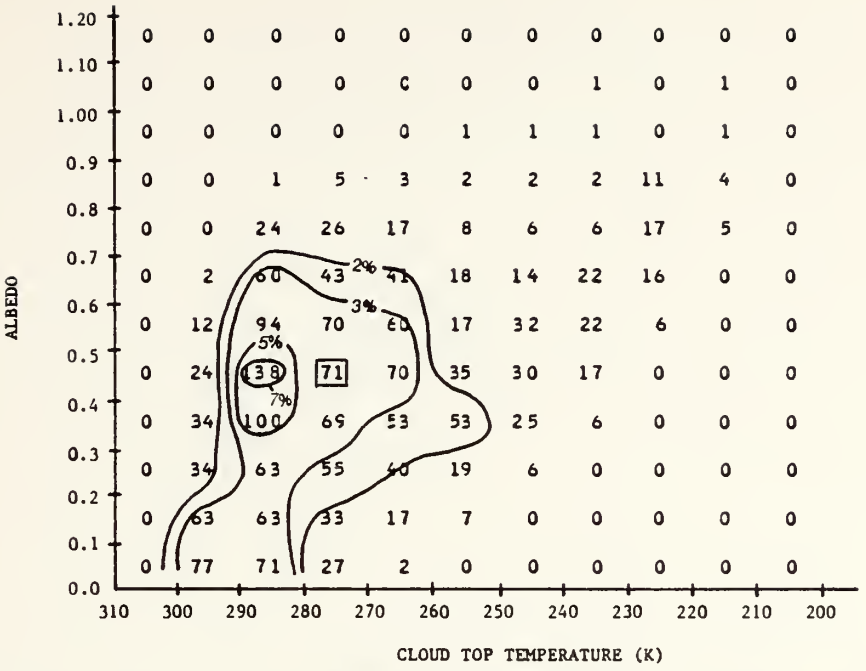

Figure 15. Nc-Precipitation Overcast Data for 10 x 10 Array Size (The mean, .407 and 272.6K, interval is boxed. The 2%, 3%, 5% and 7% frequencies are for 40, 59, 99, and 138 occurrences, respectively.)

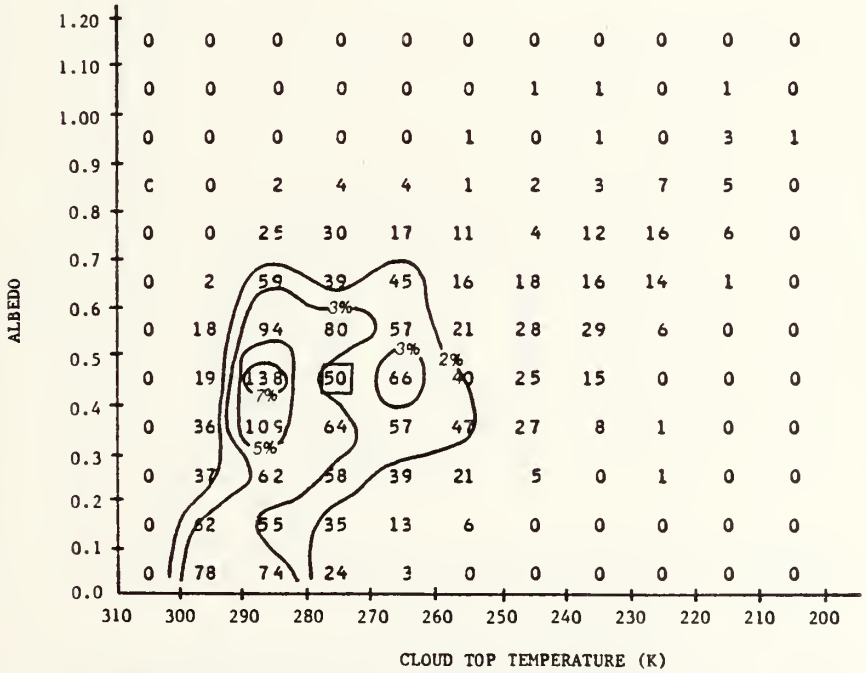

Figure 16. No-Precipitation Overcast Data for 8 x 8 Array Size (The mean, .411 and 272.5K, interval is boxed. The 2%, 3%, 5% and 7% frequencies are for 40, 59, 99, and 138 occurrences, respectively.)

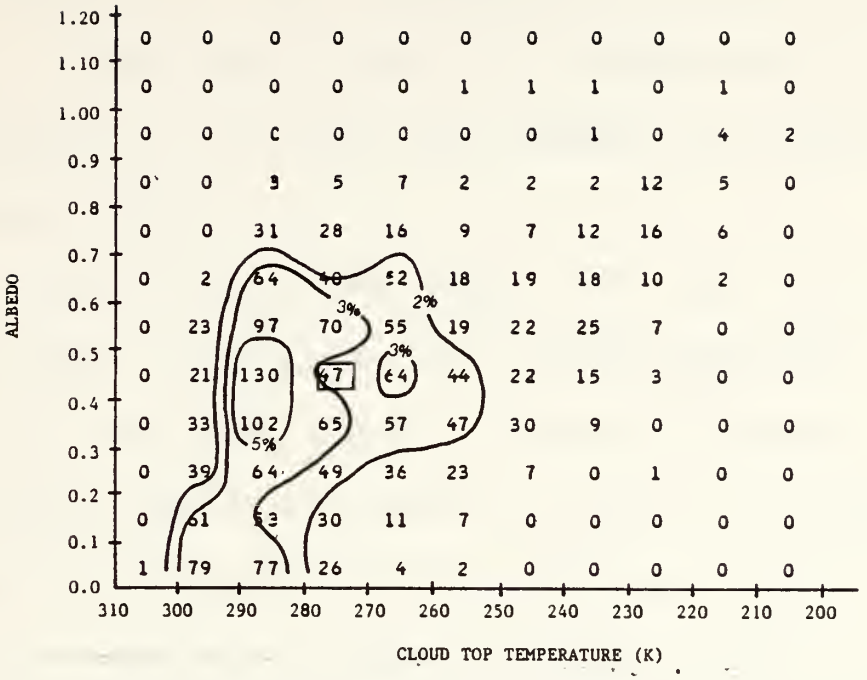

Figure 17. No-Precipitation Overcast Data for 6 x 6 Array Size (The mean, .415 and 272.4K, interval is boxed. The 2%, 3%, and 5% frequencies are for 40, 59, and 99 occurrences, respectively.)

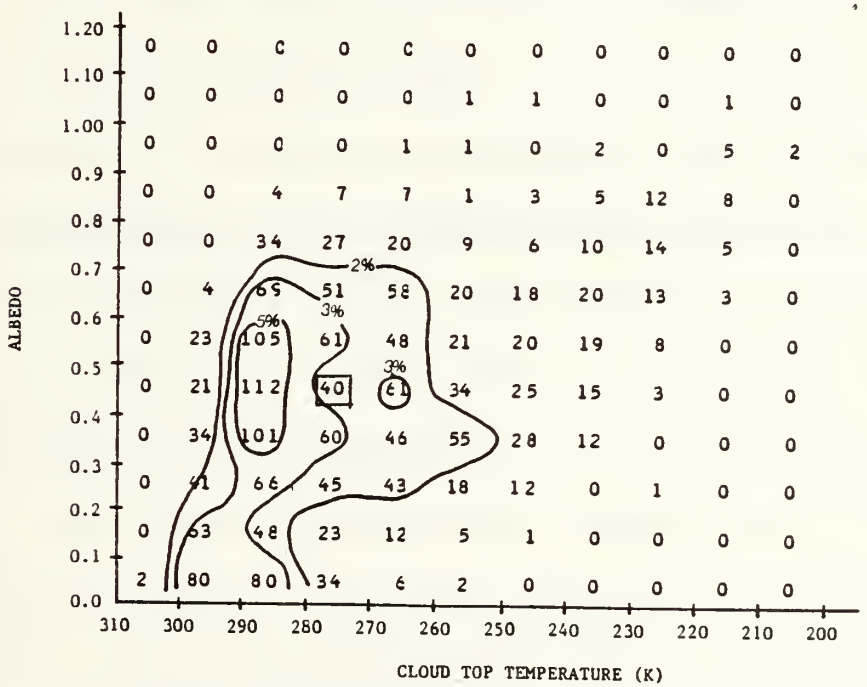

Figure 18. No-Precipitation Overcast Data for 4 x 4 Array Size (The mean, .418 and 272.3K, interval is boxed. The 2%, 3%, and 5% frequencies are for 40, 59, and 99 occurrences, respectively.)

trends discussed in the precipitation section (IV.B.1.). However, in these data, there is a greater similiarity in the statistics for the four sizes because the ceilings are all overcast reports.

The distributions (Figs. 15, 16, 17, and 18) provide visual confirmation of the similiarities between each of the four array sizes. With the exception of the second relative maxima at albedos of 0.30 to 0.40 and cloud top temperatures of 260K to 270K appearing in the 8 x 8, 6 x 6, and 4 x 4 array sizes (Figs. 16, 17, and 18), the four distributions are nearly identical. Because there are statistical differences and distributional differences in the four array sizes, the 10 x 10 and 4 x 4 arrays sizes will be used to represent the two no-precipitation data categories.

3. Precipitation and No-precipitation Comparison

The possibility arises that statistical differences in the four resolution sizes might be sufficient, or at least complement other information, in delineating the precipitation from the no-precipitation weather condition. The question then becomes, is there a statistic associated with variation of the array size within Tables X and XI which differentiates the precipitation reports from the no-precipitation overcast reports?

If the satellite data processor can vary the resolution size, as was done in this study by simply averaging different pixel array sizes, a trend in the visual and infrared data might be used to differentiate these two weather conditions. The most significant trend difference in the precipitation data (Table X) and no-precipitation overcast data (Table XI) occurs in the mean of the means. Recall that the mean of the means precipitation visual difference between the 10 x 10 and 4 x 4 array sizes was 0.035 while the no-precipitation overcast visual difference was 0.011. Similiarly the infrared differences were 2.2K and 0.3K for the precipitation and no-precipitation overcast, respectively. The precipitation data show a greater upward trend toward higher albedos and colder cloud top temperatures than the no-precipitation overcast with the finer satellite resolution.

Differentiation between these two data sets based on a comparison of the trend in the mean of the means are suggested by Tables X and XI. It must be emphasized that these tables are based on many reports and therefore reflect the most typical values. Individual reports within a given interval should be studied to provide conclusive evidence as

to whether these statistics can be used on a few reports to differentiate precipitation from no-precipitation overcast reports.

C. PRECIPITATION SPECIFICATION

An essential difference between this specification study and most of those in the literature is that the distributions of the precipitation and no-precipitation data sets are examined in detail to extract information about the probability of correct classifications. Only Lovejoy and Austin (1979) present their data distributions. The bi-spectral and life history method thresholds (Tables I and VII) refer to the typical or most common threshold values for precipitation, which is assumed to be equivalent to the mean of the means in this study. Therefore, the mean of the means can be compared to the threshold values in Tables I and VII. Additionally, a bi-spectral threshold can be proposed based on the distributions and with these distributions the amount of overlap, or the percentage of correctly classified precipitation or no-precipitation cases, can be calculated.

1. Overcast Ceilings

Are the precipitation overcast (category 1A) and no-precipitation overcast (category 2A) data sets sufficiently separated to allow differentiation of the two populations? If so, how much overlap is there between the two data sets?

a. Mean of the Means

The mean of the means statistics for the precipitation overcast versus no-precipitation overcast data, Table XII, show there is a .242 and 24.4K difference between the two populations for the 10 x 10 array size and a .254 and 25.9K difference for the 4 x 4 array size. The respective differences are greater than one standard deviation of the means of either of the two populations.

If the two precipitation overcast array sizes are compared to the no-precipitation overcast array sizes, the stronger trend in the mean of the means (Table XII) is seen in the precipitation overcast data. While the precipitation visual and infrared values vary by 0.023 and 1.8K between the 10 x 10 and 4 x 4 array sizes, the no-precipitation visual and infrared values vary by 0.011 and 0.3K. Both the mean of the means and their trends can be used to

TABLE XII

Precipitation Specification Overcast Ceilings

		Precipitation 10 x 10	No-Precipitation 10 x 10	Precipitation 4 x 4	No-Precipitation 4 x 4
Mean of Means	(VIS)	.649	.407	.672	.418
	(IR)	248.2K (-25°C)	272.6K (-1°C)	246.4K (-27°C)	272.3K (-1°C)
Standard Deviations of Means	(VIS)	.186	.205	.201	.219
	(IR)	18.9K	17.8K	19.8K	18.6K
Mean of Standard Deviations	(VIS)	.152	.122	.108	.087
	(IR)	8.9K	5.4K	4.4K	2.9K
Standard Deviation of the Standard Deviations	(VIS)	.078	.056	.069	.049
	(IR)	6.3K	4.8K	4.0K	3.1K

differentiate precipitation from no-precipitation for a large number of reports in a region similiar to this summer-time convective shower dominated area.

b. Mean of the Standard Deviations

The visual and infrared means of the standard deviations vary by 0.030 and 3.5K for the 10 x 10 array size and by 0.021 and 1.5K for the 4 x 4 array size. In the infrared values, the no-precipitation mean of the standard deviations have a magnitude 60% of the precipitation values

and produce relatively large differences. In the visual values, the no-precipitaticn mean of the standard deviations have a magnitude 80% of the precipitation values. The relatively large differences (cnly the mean of the means have a larger difference) suggest the use of this statistic to differentiate precipitation overcast from no-precipitation overcast.

c. Standard Deviation of the Means

The differences in the standard deviations of the means (Table XII) are nearly equal when comparing the two 10 x 10 array sizes and the two 4 x 4 array sizes. The visual differences are 0.019 for the 10 x 10 and 0.018 for the 4 x 4 array size. Similiarly, the infrared differences are 1.1K for the 10 x 10 and 1.2K for the 4 x 4 array size. The differences in the 4 x 4 array size (0.018 and 1.2K) are comparable to the relatively significant differences in the means of the standard deviations (.021 and 1.5K). However, the differences are not comparable in the 10 x 10 array size.

d. Standard Deviation of the Standard Deviations

The differences in the standard deviations of the standard deviations (Table XII) for the two array sizes

are approximately equal also. The visual differences are 0.022 for the 10 x 10 and 0.020 for the 4 x 4 array size. The infrared differences are 1.5K for the 10 x 10 and 0.9K for the 4 x 4 array size. Once again the differences in the 4 x 4 array size (0.020 and 0.9K) are approximately equal to the differences in the means of the standard deviations (0.021 and 1.5K), particularly in the visual value.

e. Distribution Discussion

The distributions for the 10 x 10 array size precipitation overcast (Fig. 19) and no-precipitation overcast (Fig. 15) and the 4 x 4 array size precipitation overcast (Fig. 20) and no-precipitation overcast ((Fig. 18) allow visual confirmation of the degree of separation of these two populations. These figures verify the separation between the the occurrence maxima of the two populations while showing that there is overlap of some of the values in the two populations.

The appearance of a bimodal distribution in the relatively fine resolution 4 x 4 array size precipitation overcast (category 1A) and no-precipitation overcast (category 2A) in Figs. 20 and 18 cannot be explained in terms of the precipitation categories (Table IX) or ceiling cover.

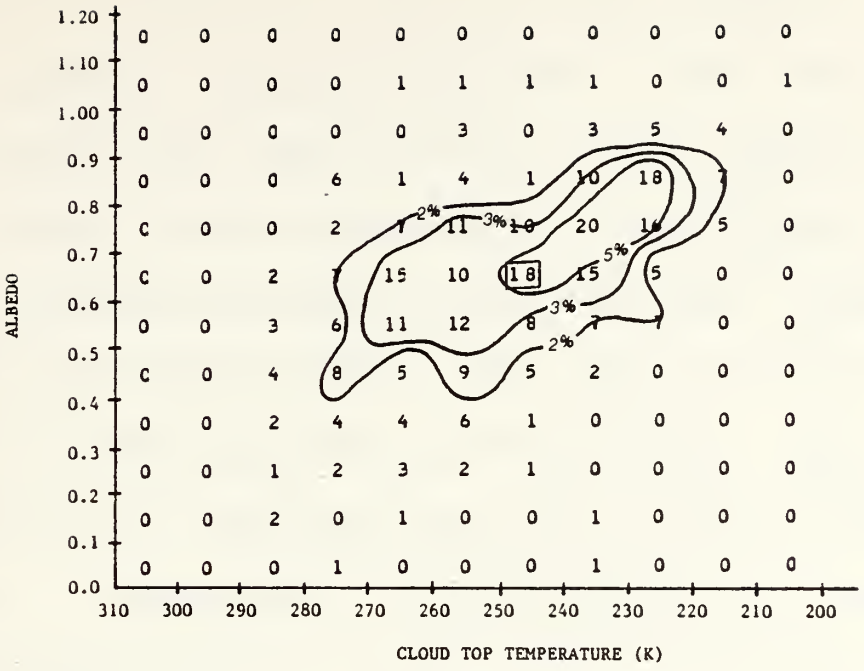

Figure 19. Precipitation Overcast Data for the 10 x 10 Array Size (The mean, .649 and 248.2K, interval is boxed. The 2%, 3%, and 5% frequencies are for 7, 10, and 16 occurrences, respectively.)

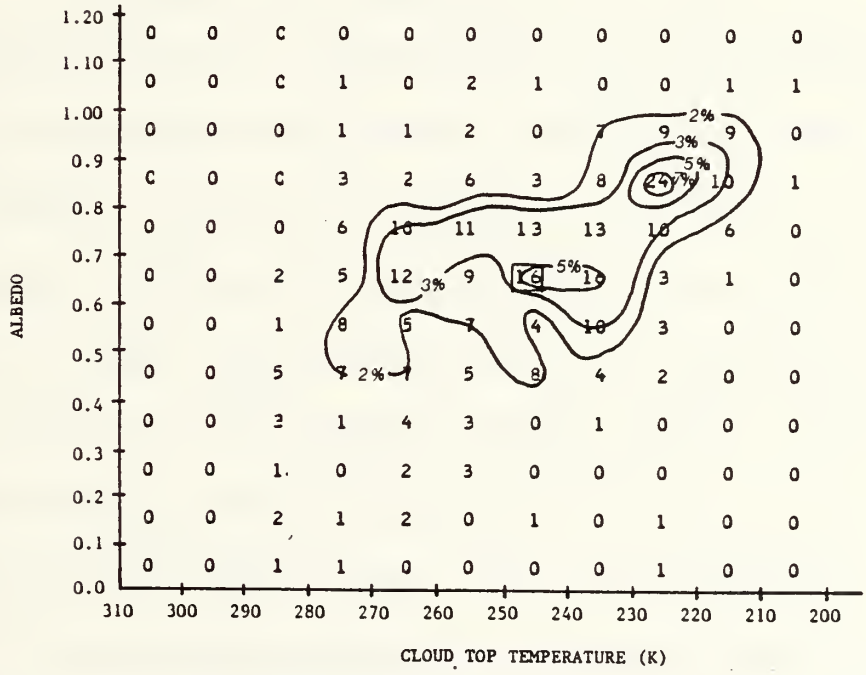

Figure 20. Precipitation Overcast Data for 4 x 4 Array Size (The mean, .672 and 246.4K, interval is boxed. The 2%, 3%, 5% and 7% frequencies are for 7, 10, 16, and 23 occurrences, respectively.)

An alternate explanation might be that these two maxima reflect different synoptic signatures. Four weak frontal systems impact this data set region during August 1979 and cause a change in the cloudiness and precipitation pattern which is normally produced by daytime heating. Recall that the Lovejoy and Austin (1979) data set also showed bimodal distributions for the cumulus no-rain reports. The bimodal distributions in this study may not be due to a synoptic signature. Nonetheless, this possibility should be investigated.

f. Precipitation Probabilities

Precipitation probabilities (Figs. 21 and 22) were computed from the precipitation overcast (category 1A) and the no-precipitation overcast (category 2A) data for the 10 x 10 (Figs. 19 and 15) and the 4 x 4 (Figs. 20 and 18) array sizes. Estimated albedos greater than 1.00 were not included in these probabilities as they accounted for only two and three no-precipitation overcast reports and four and five precipitation overcast reports in the 10 x 10 size and 4 x 4 array size, respectively. The two probability figures indicate that the 50% probability of precipitation is not a simple function of mean albedo and mean cloud top temperature.

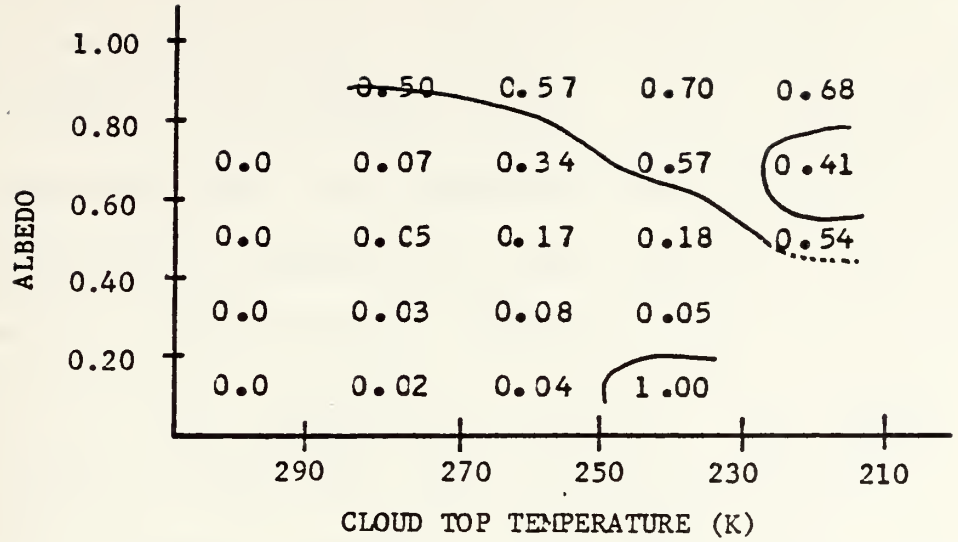

Figure 21. Precipitation Overcast Data Probability 10 x 10 Array Size

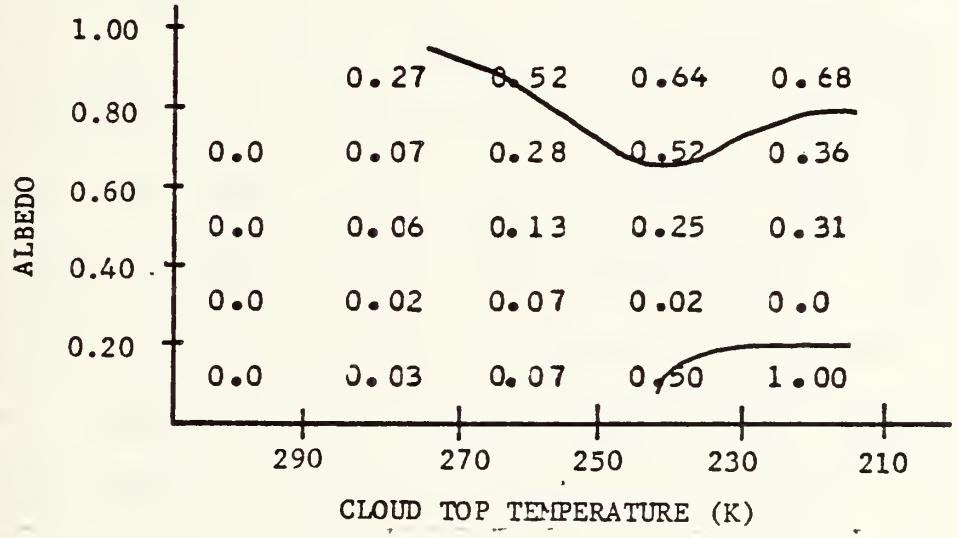

Figure 22. Precipitation Overcast Data Probability 4 x 4 Array Size

The 50% probability line (Fig. 21) shows the precipitation at low cloud top temperatures (270K-290K)

occurs at high albedos (0.80-1.00) and at cold cloud top temperatures (210K-230K) occurs at relatively low albedos (0.40-0.60). One exception occurs in the 0.60-0.80 albedo and 210K-230K cloud top temperature interval and represents 26 precipitation reports of 64 total reports. The 100% precipitation probability at 0.00-0.20 albedo and 230K-250K results from two precipitation reports. Two reports in a 0.20 albedo and 20K cloud top temperature interval are not a sufficient number of reports to be a significant indication of a high probability of precipitation. The 50% precipitation probability line (Fig. 22) in the 4 x 4 array size data shows the same general trend of decreasing albedo with decreasing cloud top temperatures. In this fine resolution data (Fig. 22), there is an upturning of the 50% probability line at the coldest cloud top temperatures, 210K-230K. There are 73 no-precipitation overcast and 80 precipitation overcast reports in the 4 x 4 array size data in the 210K-230K interval so the upturning is not the result of lack of data. The appearance, once again, of a greater than 50% probability of precipitation at low albedos, 0.00-0.20, between 210K-250K results from a total of four reports (one precipitation report of two total reports in the 230K-250K

interval and two precipitation reports of two reports in the 210K-230K) and is not a significant indication of high precipitation probability.

If a straight line is drawn to represent the 50% probability line, the lines for the two array sizes are nearly coincident until the 230K cloud top temperature is reached. For the purposes of this study, a simple linear function bi-spectral precipitation threshold based on a 50% probability of precipitation can be approximately defined as extending from 1.00 albedo and 290K cloud top temperature to 0.60 albedo and 210K cloud top temperature.

Comparison of this linear bi-spectral threshold with the Muench and Keegan (1979) threshold (Fig. 2), shows the proposed threshold has an albedo approximately 0.10 smaller at corresponding cloud top temperatures. The 50% probability asymptote at the warm cloud top temperatures shown in the Muench and Keegan (1979) results (Fig. 2), are not shown in Figs. 21 and 22 due to lack of reports in these values. The lower albedo values for this linear bi-spectral threshold may be associated with the dominance of convective precipitation (426 of 538 reports) in the precipitation data. The effect of convective precipitation reports on the satellite albedo values is discussed in Section IV.D.

g. Summary

The two significant statistics for precipitation specification of overcast ceiling reports for both array sizes are the mean of the means and the mean of the standard deviations (Table XII). The probabilites in Figs. 21 and 22 make use of the mean of the means only. Inclusion of the mean of the standard deviations in the precipitation and no-precipitation distribution plots may more distinctly define the two weather data types. The question is, how to graphically display four variables (i.e. four dimensions) in one plot?

One solution is to find a three-dimensional plot that involves the four variables. The most straight forward approach is to define the 50% probability for the mean of the means (Figs. 21 and 22) in terms of a surface. A plane would be the simplest surface choice. The equation of a line perpendicular to the 50% probability plane intersecting its midpoint in the distribution planes shown would then be calculated. All of the precipitation and no-precipitation points would be projected onto the line and the line would become the x-axis in a new plot. Thus this x-axis reflects the visual and infrared mean of the means. The visual and

infrared mean of the standard deviations would define the y-axis and z-axis, respectively.

The defined plot for the precipitation and no-precipitation data would show the relative dependence of the data on the four variables. If the plots produced distinct groups for the precipitation and no-precipitation data, new precipitation probabilities would be calculated. The variation with satellite resolution size of the precipitation probabilities would then have to be reconsidered with the new data. The data processing described is beyond the scope of this particular research effort and is recommmended for future investigation.

Precipitation specification for overcast ceilings can be delineated by the values for the mean of the means and the mean of the standard deviations for any array size discussed in this study. The mean of the mean values when used with Figs. 21 and 22 will indicate the probability of precipitation, given a similiar time of year and climatological area. A simple linear bi-spectral threshold, based on a 50% probability of precipitation, is defined approximately as extending from a 1.00 albedo and a 290K cloud top temperature to a 0.60 albedo and a 210K cloud top temperature.

2. Overcast and Broken Ceilings

Once again the question arises, are the precipitation overcast and broken (category 1B) and no-precipitation overcast and broken (category 2B) data sets sufficiently separated to allow differentiation of the two populations? If so, how much overlap is there between the two data sets?

a. Mean of the Means

The mean of the means statistics for the precipitation overcast and broken (category 1B) versus no-precipitation overcast and broken (category 2B) data, Table XIII, show there is a .309 and 27.0K difference between the two populations for the 10 x 10 pixel size and a .339 and 29.1K difference for the 4 x 4 pixel size. The respective differences are approximately equal to one and one-half standard deviations of the means of either of the two populations.

For these data, the differences in the trends of the mean of the means between the 10 x 10 and 4 x 4 array sizes for the precipitation overcast and broken reports are more dramatic than for the precipitation overcast reports. There is a 0.036 visual and a 2.2K infrared difference in the precipitation overcast and broken data and only a 0.006 visual and a 0.1K in the no-precipitation overcast and

TABLE XIII

Precipitation Specification Overcast and Broken Ceilings

		Precipitation 10 x 10	No-Precipitation 10 x 10	Precipitation 4 x 4	No-Precipitation 4 x 4
Mean of Means	(VIS)	.580	.271	.616	.277
	(IR)	252.8K (-20°C)	279.8K (+7°C)	250.6K (-23°C)	279.7K (+7°C)
Standard Deviations of Means	(VIS)	.210	.189	.225	.207
	(IR)	20.5K	16.6K	21.5K	17.8K
Mean of Standard Deviations	(VIS)	.173	.128	.124	.094
	(IR)	10.4K	5.9K	5.6K	3.2K
Standard Deviation of the Standard Deviations	(VIS)	.078	.064	.072	.057
	(IR)	7.0K	5.7K	4.9K	3.7K

broken data between the 10 x 10 and 4 x 4 array sizes. Therefore, variation of the resolution size and the trend for the mean of the means can be used, as well as the mean of the means value itself, in delineating precipitation from no-precipitation for these overcast and broken ceiling reports.

b. Mean of the Standard Deviations

The values of the mean of the standard deviations are important. The 0.045 albedo and 4.5K cloud top

temperature difference between the two data sets for the 10 x 10 array size are significant as well as the 0.030 and 2.4K difference for the 4 x 4 array size.

c. Standard Deviations of the Means

The differences in the standard deviations of the means are nearly equal when comparing the two 10 x 10 array sizes and the two 4 x 4 array sizes. The visual differences are 0.021 for the 10 x 10 and 0.018 for the 4 x 4 array size. Similiarly, the infrared differences are 3.9K for the 10 x 10 and 3.7K for the 4 x 4 array size. The visual differences are 40% less than the statistically significant visual mean of the standard deviation differences and the infrared differences are comparable to the infrared mean of the standard deviation differences.

d. Standard Deviation of the Standard Deviations

The differences in the standard deviations of the standard deviations are approximately equal. The visual differences are 0.014 for the 10 x 10 and 0.015 for the 4 x 4 array size. The infrared differences are 1.3K for the 10 x 10 and 1.2K for the 4 x 4 array size. Both the visual and infrared differences are 50% less than the respective significant differences in the mean of the standard deviations.

e. Distribution Discussion

The distributions for the 10 x 10 array size precipitation cvercast and broken (Fig. 23) and no-precipitaticn overcast and broken (Fig. 24) and the 4 x 4 array size precipitation overcast and broken (Fig. 25) and no-precipitation cvercast and broken (Fig. 26) allow visual confirmation of the relatively larger degree of separation between these two populations compared to the overcast ceiling data. These figures once again also show overlap between the two populations.

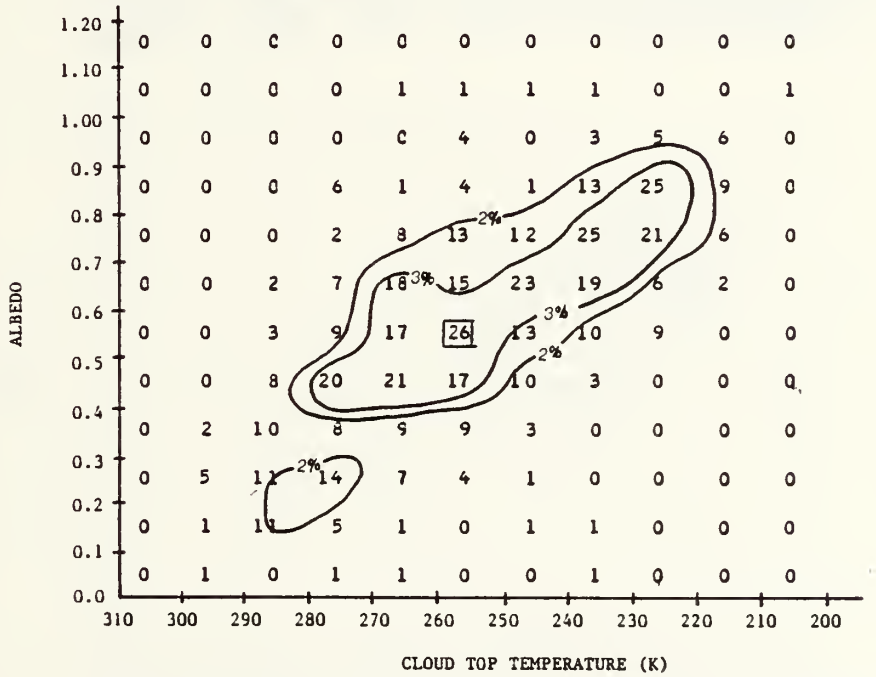

Figure 23. Precipitation Overcast and Broken Data for 10 x 10 Array (The mean, .580 and 252.8K, interval is boxed. The 2% and 3% frequencies are for 11 and 16 occurrences, respectively.)

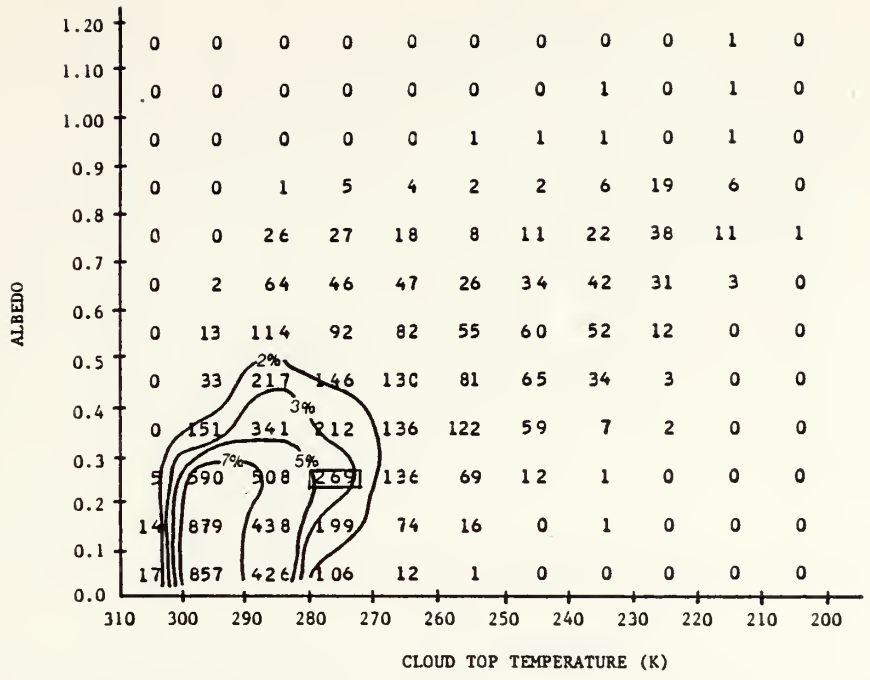

Figure 24. No-Precipitation Overcast and Broken for 10 x 10 Array (The mean, .271 and 279.8K, interval is boxed. The 2%, 3%, 5%, and 7% frequencies are for 147, 221, 368, and 515 occurrences, respectively.)

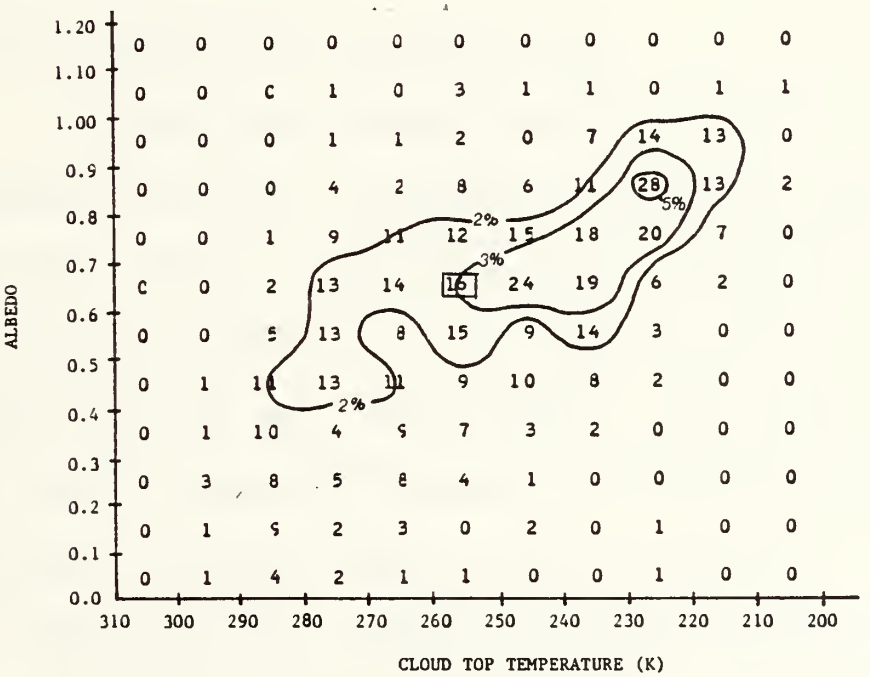

Figure 25. Precipitation Overcast and Broken Data for 4 x 4 Array (The mean, .616 and 250.6K, interval is boxed. The 2%, 3%, and 5% frequencies are for 11, 16, and 27 occurrences, respectively.)

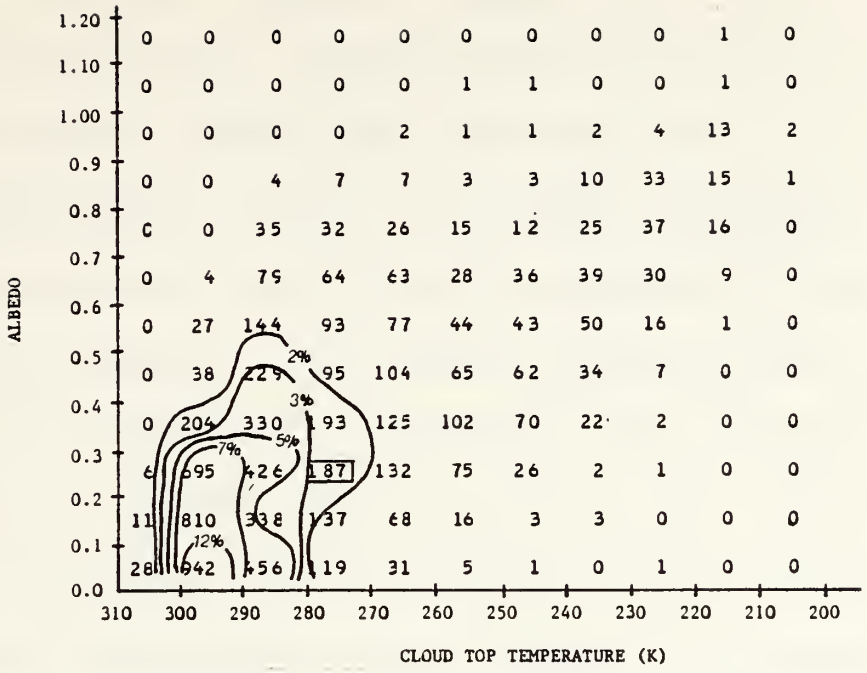

Figure 26. No-Precipitation Overcast and Broken for 4 x 4 Array (The mean, .277 and 279.7K, interval is boxed. The 2%, 3%, 5%, 7%, and 12% frequencies are for 147, 221, 368, 515, and 883 occurrences, respectively.)

f. Precipitation Probabilities

Precipitation probabilities (Figs. 27 and 28) were computed from the precipitation overcast and broken (category 1B) and the no-precipitation overcast and broken (category 2B) data for the 10 x 10 (Figs. 23 and 24) and the 4 x 4 (Figs. 25 and 26) array sizes. As in the overcast ceiling reports, there is a greater than 50% probability of precipitation at the low albedo values, 0.00-0.20. In Fig. 27, the 75% probability between 230K-250K interval results from three precipitation reports of four total reports. The

overcast ceiling reports account for two of the precipitation reports. Therefore, one precipitation and one no-precipitation broken report have been added to the interval. Similiarly in Fig. 28, the 67% probability in the 210K-230K interval results from two precipitation reports of three total reports. The overcast ceiling reports account for two of the precipitation reports. Thus, one no-precipitation report has been added to the interval. A few reports in these low albedo and cold cloud top temperature intervals are producing misleadingly high precipitation probabilities. The 50% probability line is nearly constant, at a 0.80 albedo, at all cloud top temperatures for the overcast and broken ceiling data.

The same treatment for displaying the four variables in a three dimensional diagram suggested in the previous section (IV.C.1.), is recommended for these data as well. The new displays then could be used to calculate precipitation probabilities that might allow a more accurate bi-spectral threshold specification of precipitation.

g. Summmary

As for the overcast ceilings, precipitation specification of the overcast and broken ceilings can be

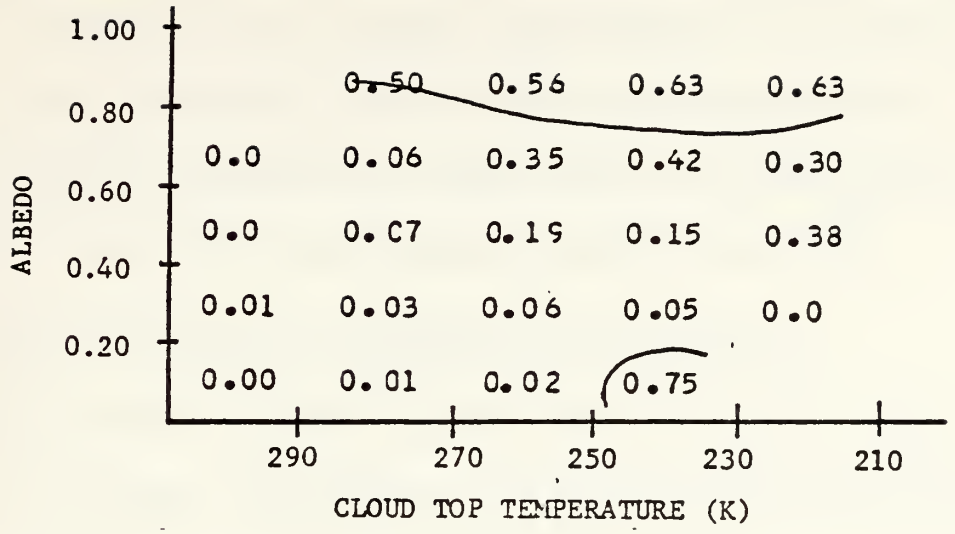

Figure 27. Precipitation Data Probability 10 x 10 Array Size (Overcast and Broken Ceilings)

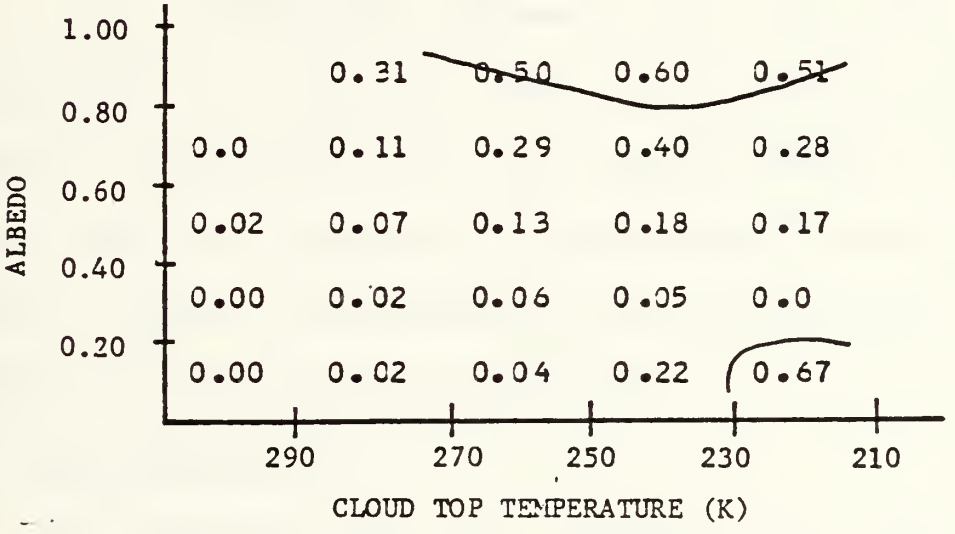

Figure 28. Precipitation Data Probability 4 x 4 Array Size (Overcast and Broken Ceilings)

delineated by the values for the mean of the means and the mean of the standard deviations for any array size discussed

in this study. The mean of the means values when used with Figs. 27 and 28 will indicate the probability of precipitation, given a similiar time of year and climatological area. A very simple threshold for these data is actually dependent upon the visual data value being greater than 0.80.

D. CONVECTIVE VERSUS CONTINUOUS PRECIPITATION

The physical processes involved in convective precipitation, or showers, are different from those processes usually involved in continuous precipitation. The inherent differences in the processes might result in a statistical separation in the thresholds between the two types of precipitation. For this data set, 426 of the 538 cases are classified as convective by the surface weather report. With the data set consisting of southeastern United States stations in August, the dominance of the precipitation cases by convective reports is not surprising.

1. Mean Statistics

The statistics for the convective and continuous precipitation (Table XIV) indicate differences in the means of the cell means of .013 and 5.7K for the 10 x 10 array size and differences of .015 and 6.8K for the 4 x 4 array size. As mentioned in the life history methods, convective

precipitation is expected to be associated with relatively higher albedos and colder cloud top temperatures. For these data, the convective precipitation are associated with colder cloud top temperatures resulting from the cumulonimbus clouds.

TABLE XIV

Continuous versus Convective Precipitation Specification

		Continuous 10 x 10	Convective 10 x 10	Continuous 4 x 4	Convective 4 x 4
Mean of Means	(VIS)	.589	.576	.602	.617
	(IR)	257.5K (-16°C)	251.8K (-21°C)	256.2K (-17°C)	249.4K (-24°C)
Standard Deviations of Means	(VIS)	.201	.214	.221	.228
	(IR)	19.4K	20.8K	20.1K	21.9K
Mean of Standard Deviations	(VIS)	.147	.180	.099	.131
	(IR)	7.6K	11.1K	3.8K	6.0K
Standard Deviation of the Standard Deviations	(VIS)	.075	.078	.058	.075
	(IR)	5.3K	7.2K	3.2K	5.2K

The statistics for the convective and continuous precipitation (Table XIV) suggest that for visual satellite values, the mean of the standard deviations is the best statistic for differentiation of these two data types, while

for infrared values, the mean of the means is the best statistic. The use of two different statistical types to qualitatively specify continuous precipitation from convective precipitation is unique to this pair of convective versus continuous precipitation data comparison.

The infrared mean of the cell means show that the convective precipitation has colder cloud top temperatures due to the greater vertical development of the clouds. The greater vertical variation of the convective precipitation clouds is seen in the visual "texture" or visual mean of the standard deviation statistics. This "texture" difference also appears in the infrared values, but it is not as significant as the differences in the infrared mean of the means. The lack of a large difference in the visual mean of the means between the convective and continuous precipitation reflects the averaging of open areas and cumulus clouds associated with convective precipitation. Note that for the fine resolution 4 x 4 array size, the visual mean of the means is larger for the convective than the continuous precipitation.

The visual means of the standard deviations have a difference of 0.033 for the 10 x 10 and 0.032 for the 4 x 4

array size. Contrast these difference to the visual mean of the mean differences of 0.013 and 0.015 for the 10 x 10 and 4 x 4 array size, respectively. The infrared mean of the means have a difference of 5.7K for the 10 x 10 and 6.8K for the 4 x 4 array size. These differences are larger than the infrared mean of the standard deviations differences of 3.5K for the 10 x 10 and 2.2K for the 4 x 4 array size.

2. Standard Deviation Statistics

The standard deviation of the means and the standard deviation of the standard deviations display quite similiar and relatively insignificant differences. The visual standard deviation of the means vary by 0.013 in the 10 x 10 and 0.007 in the 4 x 4 with the infrared values varying by 1.4K for the 10 x 10 and 1.8K for the 4 x 4 array sizes. The visual and infrared 10 x 10 and 4 x 4 array size differences in the standard deviations of the standard deviations are 0.003, 0.017, 1.9K, and 2.0K, respectively.

3. Distribution Discussion

The distributions of the convective and continuous precipitation for the 10 x 10 array size (Figs. 29 and 30) and for the 4 x 4 array size (Figs. 31 and 32) demonstrate the similiarity of the distributions. This similiarity

disallows quantitative separation of the convective and continuous precipitation.

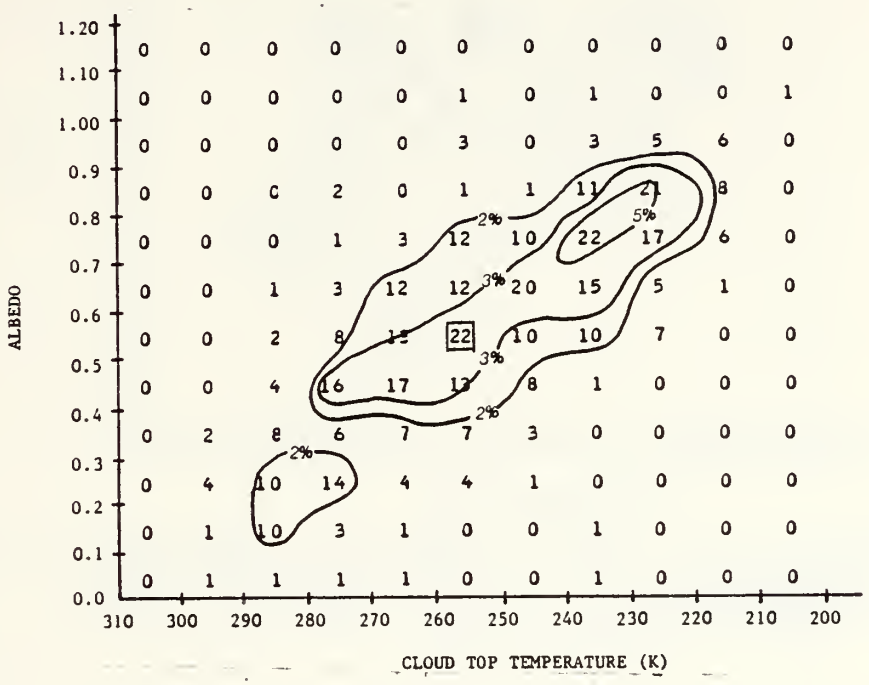

Figure 29. Convective Precipitation Data for 10 x 10 Array Size (The mean, .576 and 251.8K, interval is boxed. The 2%, 3%, and 5% frequencies are for 9, 13, and 21 occurrences, respectively.)

4. Summary

Defining the qualitative delineation of convective versus continuous precipitation in terms of the shift toward colder cloud top temperatures for the convective precipitation cases is one available delimiter. The second qualitative separation is in terms of the shift toward higher albedo values of the mean of the standard deviations for the

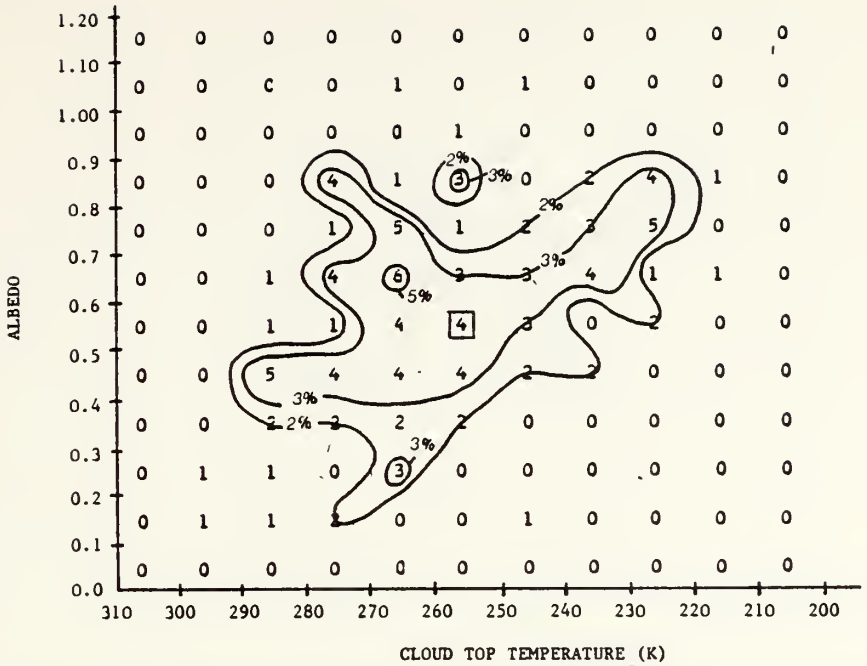

Figure 30. Continuous Precipitation Data for 10 x 10 Array Size (The mean, .589 and 257.5K, interval is boxed. The 2%, 3%, and 5% frequencies are for 2, 3, and 6 occurrences, respectively.)

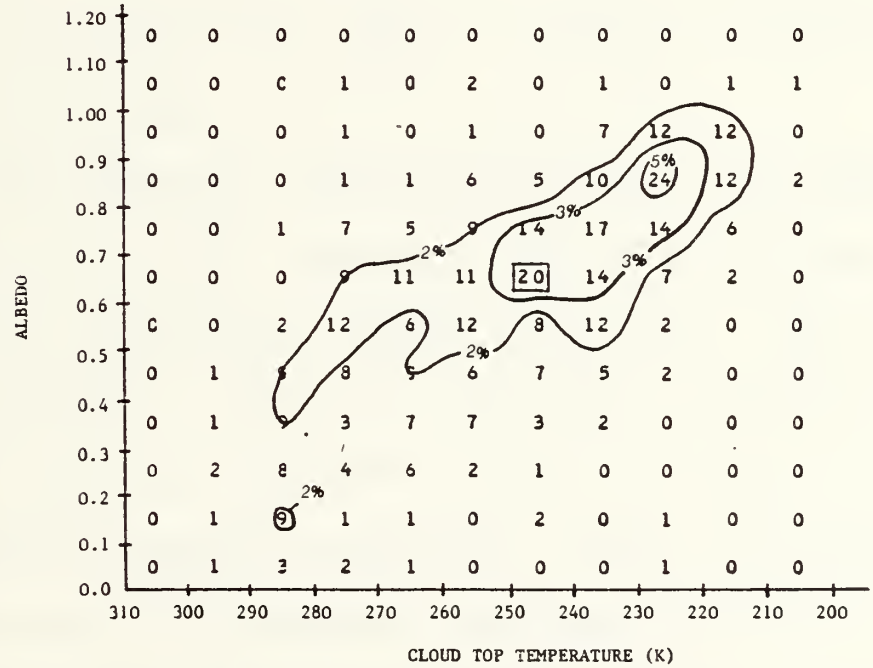

Figure 31. Convective Precipitation Data for 4 x 4 Array Size (The mean, .617 and 249.4K, interval is boxed. The 2%, 3%, and 5% frequencies are for 9, 13, and 21 occurrences, respectively.)

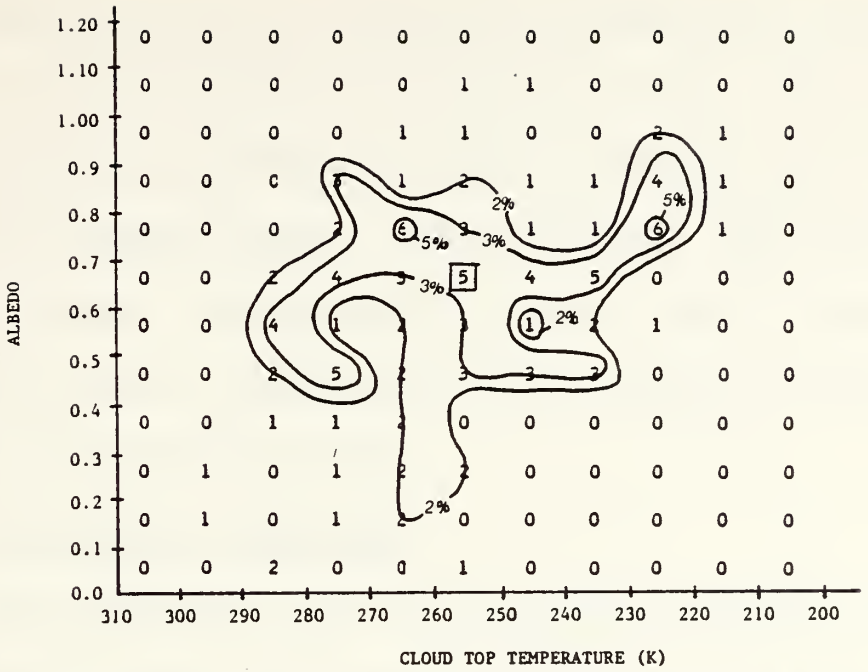

Figure 32. Continuous Precipitation Data for 4 x 4 Array Size (The mean, .602 and 256.2K, interval is boxed. The 2%, 3%, and 5% frequencies are for 2, 3, and 6 occurrences, respectively.)

convective precipitation cases as compared to the continous precipitation cases.

The convective precipitation cloud top temperature mean of 251.8K (-21°C) compares quite well with those associated with life history methods (Table VII). The continuous precipitation cloud top temperature of 257.5K (-16°C) compares well with the -16°C threshold of Wylie (1979) (a life history threshold for Montreal, Canada, in summertime) and with the -12°C bi-spectral threshold of Muench and Keegan (1979). These research efforts focused on mid-latitude precipitation associated with fronts.

E. INTENSITY

As there is little statistical difference between the convective and continuous precipitation data, the qualitative analysis of precipitation can be based strictly on all light or all moderate/heavy precipitation. The light precipitation cases are expected to have a lower mean albedo and warmer cloud top temperature when compared to the moderate/heavy precipitation cases.

1. Statistical Discussion

The statistics for the two precipitation intensities, Table XV, show 0.100 and 8.6K differences for the 10 x 10 array size and .117 and 8.1K differences for the 4 x 4 array size in the means of the means. The differences are approximately equal to one-half a standard deviation, an insufficient separation for specification of these two precipitation classifications. The remaining three sets of statistics (Table XV) show nearly identical values in the light and moderate/heavy precipitation for the two array sizes.

TABLE XV

Light versus Moderate/Heavy Precipitation Specification

		Light	Moderate/ Heavy	Light	Moderate/ Heavy
		10 x 10	10 x 10	4 x 4	4 x 4
Mean of Means	(VIS)	.565	.665	.598	.715
	(IR)	254.2K (-19°C)	245.6K (-28°C)	251.9K (-21°C)	243.8K (-29°C)
Standard Deviations of Means	(VIS)	.210	.201	.226	.204
	(IR)	20.5K	20.4K	21.6K	21.3K
Mean of Standard Deviations	(VIS)	.172	.177	.124	.129
	(IR)	10.2K	11.9K	5.5K	6.1K
Standard Deviation of the Standard Deviations	(VIS)	.078	.081	.072	.079
	(IR)	7.0K	7.0K	4.9K	5.2K

2. Distribution Discussion

The distributions of the light and moderate/heavy precipitation for the 10 x 10 (Figs. 33 and 34) and the 4 x 4 array size (Figs. 35 and 36) allow visual confirmation of the overlap between the two intensities. Basically with only 74 cases of moderate/heavy precipitation, the frequency contours (Figs. 34 and 36) reflect a noisy distribution created by a sorting of just two or three reports into a given interval. Additional intensity data, specifically

moderate/heavy precipitation cases, are needed before a threshold delineating qualitative intensities can be proposed.

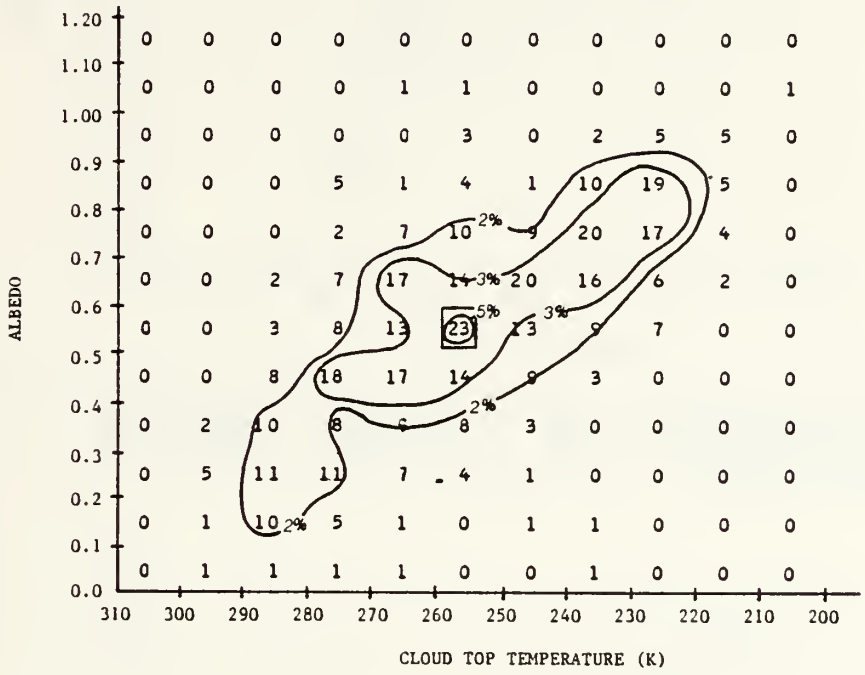

Figure 33. Light Precipitation Data for 10 x 10 Array Size (The mean, .565 and 254.2K, interval is boxed. The 2%, 3%, and 5% frequencies are for 9, 14, and 23 occurrences, respectively.)

For the 10 x 10 and 4 x 4 array sizes moderate/heavy precipitation (Figs. 34 and 36), the area encompassed by the 7% frequency isopleth at the higher albedos and colder cloud top temperatures gives an indication of a possible separation between the twc intensities. However, the bimodal nature of the 10 x 10 distribution (Fig. 34) and the

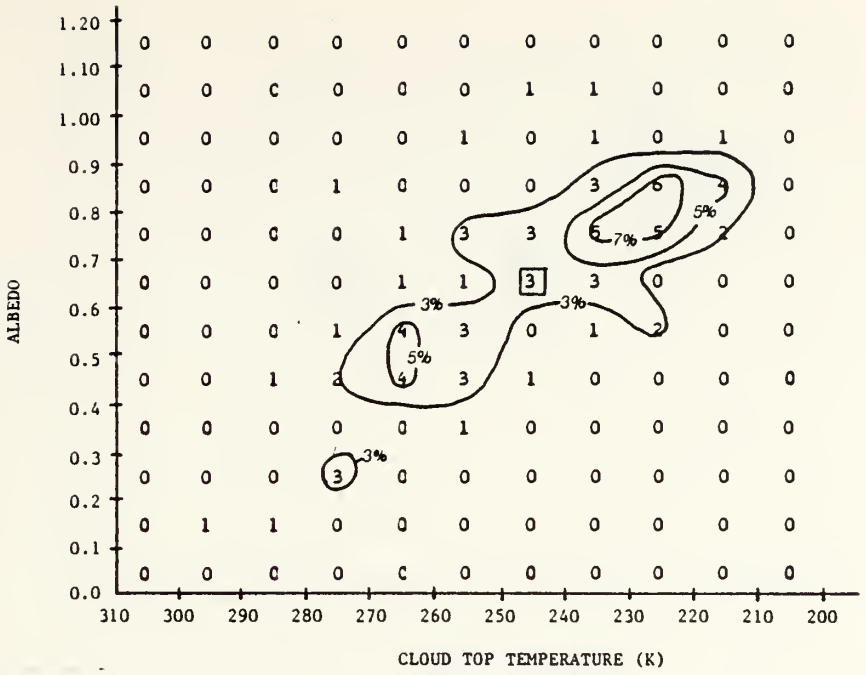

Figure 34. Moderate/Heavy Precipitation Data for 10 x 10 Array Size (The mean, .665 and 245.6K, interval is boxed. The 3%, 5%, and 7% frequencies are for 2, 4, and 5 occurrences, respectively.)

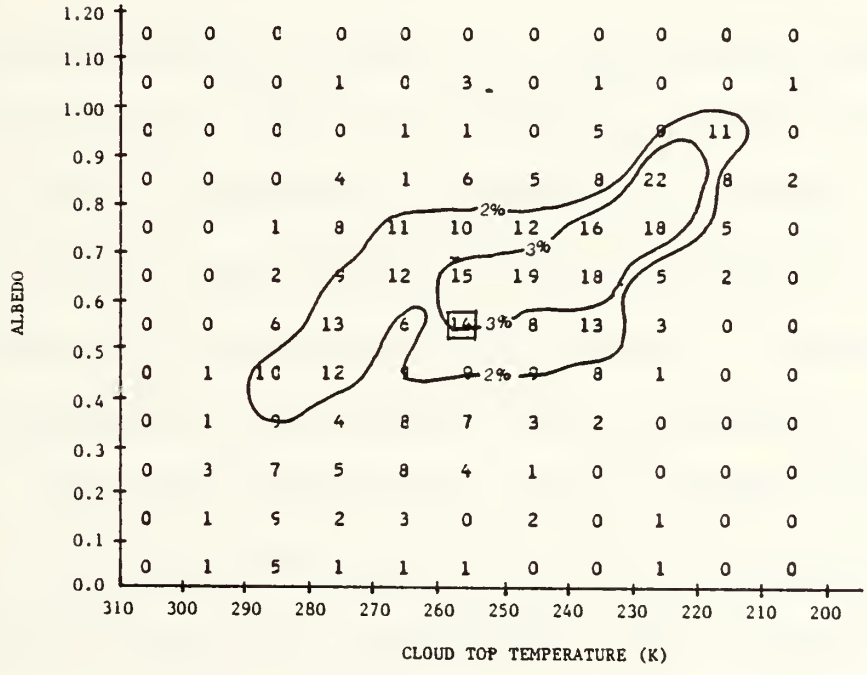

Figure 35. Light Precipitation Data for 4 x 4 Array Size (The mean, .598 and 251.9K, interval is boxed. The 2% and 3% frequencies are for 9 and 14 occurrences, respectively.)

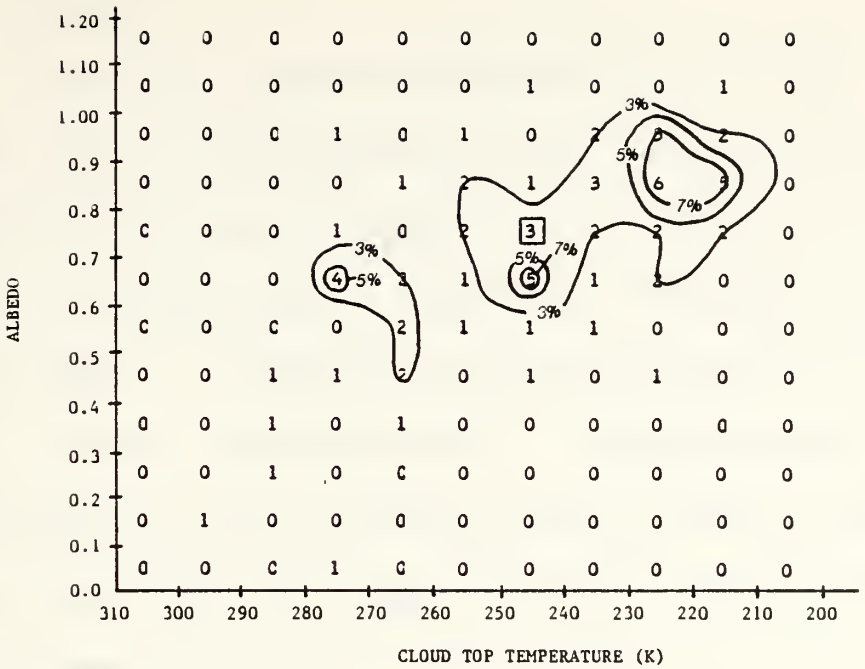

Figure 36. Moderate/Heavy Precipitation Data for 4 x 4 Array Size (The mean, .715 and 243.8K, interval is boxed. The 3%, 5%, and 7% frequencies are for 2, 4, and 5 occurrences, respectively.)

three relative maxima of the 4 x 4 distribution (Fig. 36) suggest that there will be a significant amount of overlap between these two qualitative intensities. Because the statistics for the two rainfall rates are nearly identical (Table XV), with the exception of the mean of the means, the method discussed in the precipitation specification section (IV.C.) which involved the mean of the standard deviations to aid in further differentiation of two data types cannot be applied to these two intensities. The delineation will have to be derived from the mean of the mean statistics and their resultant distributions.

3. Summary

There are slight manifestations of the expected downward shift in the albedos and the warmer cloud top temperatures for the light precipitation relative to the moderate/heavy precipitation. However, additional data are required before a threshold can be proposed to delineate light versus moderate/heavy precipitation. The investigation of the additional data should begin with consideration of the mean of the means and their distributions.

During the cell resolution discussion of Section IV.B.1., a significant number of low albedo values (less than 0.40 albedo) were noted. A comparison of the light precipitation data (Fig. 33) and precipitation data (Fig. 10) for the 10 x 10 array size reveals that 96% (105 of 109 reports) are classified as light precipitation. Further analysis shows that 79% (86 of 109 cases) are classified as light convective precipitation. (The decomposition of convective and continuous precipitation data into light and moderate/heavy are not shown.) These low albedo values are not unreasonable for light convective precipitation which can be produced by small, isolated cumulus congestus clouds.

V. SUMMARY AND CONCLUSIONS

A. DATA PROCESSING SUMMARY

The data were first filtered for the correct time, 1200-2000 GMT, to ensure reliable visual satellite values. The visual counts were converted to albedos according to the Muench and Keegan (1979) normalization scheme (see Appendix A). This scheme corrects for Lambertian scattering as well as anisotropic cloud radiation. Sorting the data according to the Service-A reports (current weather and cloud group) provided seven precipitation groups: convective, continuous, light, moderate/heavy, general, overcast ceiling, and overcast and broken ceiling precipitation and two no-precipitation groups: no-precipitation overcast and no-precipitation overcast and broken. In order to investigate the impact of satellite resolution on precipitation specification, the stated groups were subdivided into four sizes: 10 x 10 (45 x 45 nmi), 8 x 8 (36 x 36 nmi), 6 x 6 (27 x 27 nmi), and 4 x 4 (22 x 22 nmi) pixel array sizes. The means of the albedos and cloud top temperatures for each array size for each weather or cloud group were calculated. The mean values

were sorted into 10K cloud top temperature intervals and 0.10 estimated albedo intervals to provide a visual description of the distributions. The standard deviation of the means and the mean and standard deviation of the standard deviations for both albedc and cloud top temperature were also computed for each distribution.

B. STATISTICS SUMMARY

The computed mean and standard deviation of the means and the mean and standard deviation of the standard deviations for both albedo and cloud top temperature were evaluated for specification of precipitation, specification of continuous versus convective precipitation, and specification of light versus moderate/heavy precipitation.

For precipitation specification (Tables XII and XIII), the visual and infrared mean of the means produced the largest statistical differences between the precipitation and no-precipition data sets for both the overcast and the overcast and broken ceiling reports. For the overcast ceiling reports (Table XII), the separation in the visual and infrared means of the means were one standard deviation. For the overcast and broken ceiling reports (Table XIII), the separation in the visual and infrared means of the means were

one and one-half standard deviations. The mean of the standard deviations and the trend of the mean of the means also yielded a large difference between the precipitation and no-precipitation data sets.

For specification of continuous versus convective precipitation (Table XIV), the infrared mean of the means and the visual mean of the standard deviations yielded the largest statistical differences. The convective precipitation infrared mean of the means was 6K-7K colder than the continuous precipitation value and the convective visual mean of the standard deviations was 20% greater than the continuous precipitation value. These two statistics, however, were only indications of possible separation as the two data distributions displayed significant overlap.

For light versus moderate/heavy precipitation specification (Table XV), the mean of the means yielded the largest statistical differences. However, the relatively small quantitative differences (one-half standard deviation) in the visual and infrared values only provided an indication of the upward shift in albedo and the downward shift in cloud top temperature for the moderate/heavy precipitation relative to the light precipitation.

C. PRECIPITATION PROBABILITY SUMMARY

For the overcast ceiling reports, the 10 x 10 array size (Fig. 21) 50% probability line decreased linearly to lower albedos with colder cloud top temperatures, while the 4 x 4 array size (Fig. 22) 50% probability line decreased linearly to approximately 240K and then increased linearly at colder cloud top temperatures. For the overcast and broken ceiling reports, the 10 x 10 array size (Fig. 27) 50% probability line was constant at 0.80 albedo while the 4 x 4 array size (Fig. 28) 50% probability line gradually decreased linearly to approximately 240K and then gradually increased linearly at colder cloud top temperatures.

D. DATA DISTRIBUTION SUMMARY

The distributions of all seven precipitation classes and both no-precipitation classes were non-Gaussian. This result disagrees with the assertion of Lovejoy and Austin (1979) that their cumulus rain, non-cumulus rain, and non-cumulus no-rain data distributions were Gaussian. At the relatively fine resolution 4 x 4 array size, all seven precipitation classes and the no-precipitation overcast data displayed bimodal distributions while at the relatively coarse 10 x 10 array size, all displayed an unimodal distribution.

E. CONCLUSIONS

The conclusions from this study of precipitation specification are:

- Varying the satellite data resolution from 484 nmi² (4 x 4 array size) to 2025 nmi² (10 x 10 array size) results in a statistically significant difference in the representation of precipitation or no-precipitation data. Variation in the distribution functions and the characteristic means and standard deviations with increasing cell size demonstrates systematic trends which may, with further study, provide improved basis for rain detection and/or quantification.

- For overcast ceiling reports, a simple linear bi-spectral threshold based on a 50% probability of precipitation is defined as extending from an albedo of 1.00 and a cloud top temperature of 290K to an albedo of 0.60 and a cloud top temperature of 210K for overcast ceiling reports. For overcast and broken ceiling reports, a threshold based on the albedo being greater than 0.80 specifies a 50% probability of precipitation. However, the precipitation probabilities varied with the satellite resolution size.

- The precipitation and no-precipitation data sets can be differentiated by the mean of the means, the mean of the standard deviations, and the trend of the mean of the means.

- Differentiation of convective precipitation from continuous precipitation shows promise through the differences in the infrared mean of the means and through the visual mean of the standard deviations.

- Qualitative specification of light versus moderate/heavy precipitation shows some promise through a threshold based on the relative shift toward colder cloud top temperatures and higher albedos of the moderate/heavy precipitation relative to the light precipitation.

F. SUGGESTED FURTHER STUDY

The recommendations for further study are:

- The propcsed data processing that would display the visual and infrared mean and standard deviation of the means (IV.C.1.) should be investigated for both the overcast and the overcast and broken data to determine if the precipitation and no-precipitation data can be more distinctly separated.

- The appearance of bimodal distributions at the fine resolutions (6 x 6 and 4 x 4 array sizes) in the seven precipitation categories and in the no-precipitation overcast category should be investigated as a possible synoptic signature.

- Formal discriminant analysis should be applied to the relevant statistics to yield confidence levels of individual visual and infrared satellite data pairs for precipitation specification.

- The data should be further investigated at the 2 x 2 array size to analyze this resolution in representing the data.

APPENDIX A

The Muench and Keegan (1979) normalization relates the normalized reflectivity, $\tilde{r}_n$, to the varying solar angle and maximum digital counts through the reflectance term, $\tilde{r}$, and the anisotropic scattering through the χ term. Table XVI defines the symbols, Table XVII lists the geometric identity equations and Table XVIII list the normalization equations. Fig. 37 gives an example of the normalization applied to the stated location.

TABLE XVI

List of Symbols

Symbol	Description	Units
C	GOES video count number (0-63)	dimensionless
C_o	GOES video count number for perfect diffuse reflector and overhead sun	dimensionless
G	Greenwich meridian time	hours-minutes-seconds
R	Distance of earth to sun	km
R_o	Mean distance of earth to sun	km
d	Julian date	dimensionless
h	Hour angle	radians
r	Cloud reflectivity	dimensionless
γ	Arc-length observer to subsatellite point	radians
δ	Declination of the sun	radians
ζ	Zenith angle of the sun	radians
Λ	Longitude	radians
Λ_s	Longitude of subsatellite point	radians
χ	Anisotropic scattering coefficient	dimensionless
ϕ	Latitude	radians
ϕ_1	Azimuth of the sun	radians
ϕ_2	Azimuth of the satellite	radians

TABLE XVII

Basic Geometric Satellite-Earth Relationships *

Declination:

$$\delta = 0.408 \sin [(d-81) * 2\pi/365]$$

Solar distance ratio:

$$R/R_o \cong 1 - 0.167 \cos [(d-14) * 2\pi/365]$$

Hour angle:

$$h \cong \Lambda + \pi - G(\text{hours}) \times \pi/12$$

Arc-length:

$$\cos\gamma = \cos(\Lambda_s - \Lambda) \cos\Phi$$

Satellite azimuth:

$$\sin (\phi_2 - \pi) = \sin (\Lambda_s - \Lambda)/\sin\gamma$$

Solar azimuth angle:

$$\cos\zeta = \sin\Phi \sin\delta + \cos\Phi \cos\delta \cosh$$

Solar azimuth:

$$\sin\phi_1 = \cos\delta \sinh/\sin\zeta$$

*Angles in radians

TABLE XVIII

Muench and Keegan Normalization Equations *

$$\tilde{r} = (\frac{C}{C_o})^2 * \sec\zeta$$

$$\Delta\phi = |\phi_2 - \phi_1|$$

$$C_1 = \cos^2 ((\zeta - 50) * 1.8)$$

$$C_2 = 0.7 \cos ((\zeta - 22.5) * 4) * (1 - \cos\zeta)$$

$$C_3 = \cos^8 ((\Delta\phi - 70) * 1.3)$$

$$\chi \cong 1.0 + 0.05 * (1 + \cos(2*\zeta)) + 0.20 * (C_1 + C_2) * C_3$$

$$\tilde{r}_n = [1.09 - 2*(1.09 - \tilde{r} * \chi *(R/R_o)^2)/(1 + \cos^{1/2} \zeta)]$$

*Angles in degrees

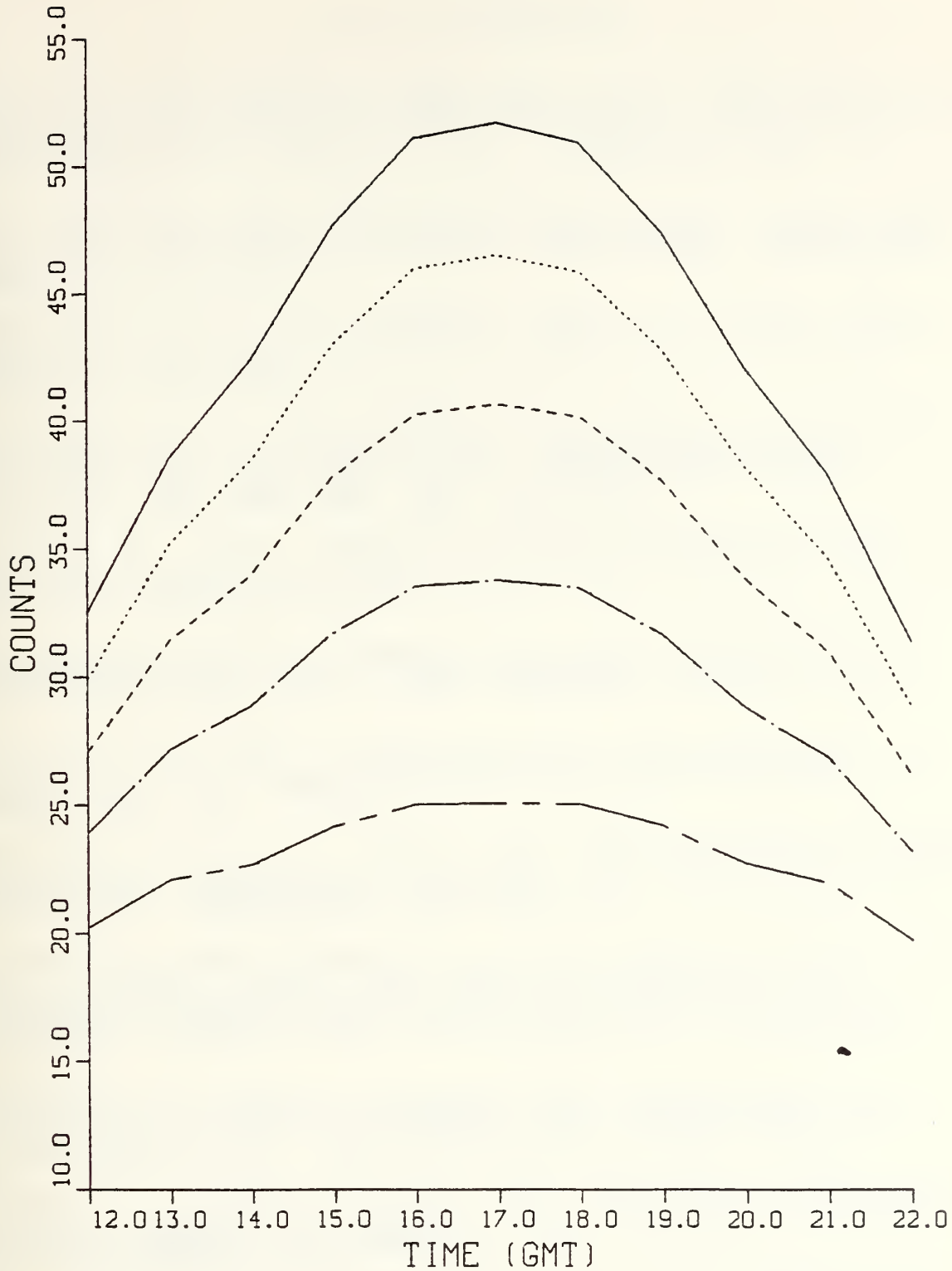

Figure 37. Normalized Cloud Reflectivity as a Function of Video Count and Time of Day for April 16 at 42°N and 74°W, with Calibration Count (C_o) equal to 60. (Example taken from Muench and Keegan, 1979.)

LIST OF REFERENCES

Coakley, J. A. and F. P. Bretherton, 1982: Cloud cover from high-resolution scanner data: detecting and allowing for partially filled fields of view. J. Geophys. Res., 87, 4917-4932.

Del Beato, R., 1981: The relationship between extratropical rainfall and satellite cloud-top temperatures. Aust. Met. Mag., 29, 125-131.

Griffith, C. G., J. A. Augustine, and W. L. Woodley, 1980: Satellite estimation in the U. S. high plains. J. Appl. Meteor., 20, 53-66.

Griffith, C. G., W. L. Woodley, P. G. Grube, D. W. Martin, J. Stout and D. N. Sidkun, 1978: Rain estimation from geosynchronous satellite imager--visible and infrared studies. Mon. Wea. Rev., 106, 1153-1171.

Liljas, E., 1981a: Analysis of cloud and precipitation through an automated classification of AVHRR data. RMK 32, SMHI (in Swedish), 33 pp.

Liljas, E., 1981b: Automated techniques for satellite imager analysis. Proc. IAMAPS Symposium, Hamburg, 25-28 Aug. 1981, 331-339.

Liou, K. N., 1976: On the absorption, reflection and transmission of solar radiation in cloudy atmospheres. J. Atmos. Sci., 33, 798-805.

Lovejoy, S. and G. L. Austin, 1979: The delineation of rain areas from visible and IR satellite data for GATE and mid-latitudes. Atmos-Ocean, 17, 77-92.

Mosher, F., 1975, Appendix to: D. W. Martin, J. Stout, and D. N. Sikdar, 1975: GATE area rain estimation from satellite images. Report, NOAA Grant 04-5-158-47, Space Science and Engineering Center, University of Wisconsin-Madison.

Muench, H. S. and T. J. Keegan, 1979: Development of techniques to specify cloudiness and rainfall rate using GOES imagery data. AFGL-TR-79-0255, AD A084, 757 pp.

Negri, A. J. and R. F. Adler, 1981: Relation of satellite-based thunderstorm intensity to radar-estimated rainfall. J. Appl. Meteor., 20, 289-300.

Platt, C. M. R., 1981: Two dimensional histogram of GMS-1 satellite visible albedo and infrared temperature for selected cloud systems. Division of Atmospheric Physics Tech. Paper No. 40, Commonwealth Scientific and Industrial Research Organization, Australia.

Scofield, R. A., 1981: Visible and infrared techniques for flash flood, hydrological, and agricultural applications. In, D. Atlas and O. W. Thiele (editors), Precipitation Measurements from Space, Workshop Report, October 1981, NASA, Goddard Space Center, Greenbelt, Md., D145-D152.

Simpson, J. and V. Wiggert, 1969: Models of precipitating cumulus towers. Mon. Wea. Rev., 89, 471-489.

Stout, J., D. W. Martin and S. N. Sikdar, 1979: Estimating GATE rainfall from geostationary satellite images. Mon. Wea. Rev., 107, 585-598.

Wylie, D. P., 1979: An application of a geostationary satellite rain estimation technique to an extratropical area. J. Appl. Meteor., 18, 1640-1648.

Wylie, D. P., 1982: Some statistics for combining radiosonde soundings with satellite images for estimting rainfall. Report, NOAA Contract NA-80-SAC-00721, Space Science and Engineering Center, University of Wisconsin-Madison.

INITIAL DISTRIBUTION LIST

		No. Copies
1.	Defense Technical Information Center Cameron Station Alexandria, VA 22314	2
2.	Library, Code 0142 Naval Postgraduate School Monterey, CA 93943	2
3.	Professor Robert J. Renard, Code 63Rd Department of Meteorology Naval Postgraduate School Monterey, CA 93943	1
4.	Professor Christopher N. K. Mooers, Code 68Mr Department of Oceanography Naval Postgraduate School Monterey, CA 93943	1
5.	Assistant Professor Carlyle H. Wash, Code 63Wy Department of Meteorology Naval Postgraduate School Monterey, CA 93943	9
6.	Assistant Professor James L. Mueller, Code 68My Department of Oceanography Naval Postgraduate School Monterey, CA 93943	1
7.	LT Linda S. Paul U. S. Naval Oceanography Command Detachment APO San Francisco, CA 96519	3
8.	Director Naval Oceanography Division Naval Observatory 34th and Massachusetts Avenue NW Washington, D.C. 20390	1
9.	Commander Naval Oceanography Command NSTL Station Bay St. Louis, MS 39522	1
10.	Commanding Officer Naval Oceanographic Office NSTL Station Bay St. Louis, MS 39522	1
11.	Commanding Officer Fleet Numerical Oceanography Center Monterey, CA 93940	1

12. Commanding Officer 1
Naval Ocean Research and Development
Activity
NSTL Station
Bay ST. Louis, MS 39522

13. Commanding Officer 1
Naval Environmental Prediction Research
Facility
Monterey, CA 93940

14. Chairman, Oceanography Department 1
U.S. Naval Academy
Annapolis, MD 21402

15. Chief of Naval Research 1
800 N. Quincy Street
Arlington, VA 22217

16. Office of Naval Research (Code 480) 1
Naval Ocean Research and Development
Activity
NSTL Station
Bay ST. Louis, MS 39522

17. Dr. Donald Wylie 1
SSEC--U. W.
1225 West Dayton Street
Madison, WI 53706

18. CAPT A. Shaffer, Code 63 1
Department of Meteorology
Naval Postgraduate School
Monterey, CA 93943

207426

Thesis
P2713
c.1

Paul

A study precipitation occurrence using visual and infrared satellite data.